# THE QUALITY OF GLACIER OBSERVATION: THE DEBRIS AREAS AND THEIR ROLE IN SIZE ESTIMATION

MUSLIM MIRZOSHOEVICH, BANDISHOEV

March, 2011

SUPERVISORS:

Ms Dr. Arta Dilo

Prof. Dr. Ir. Alfred Stein

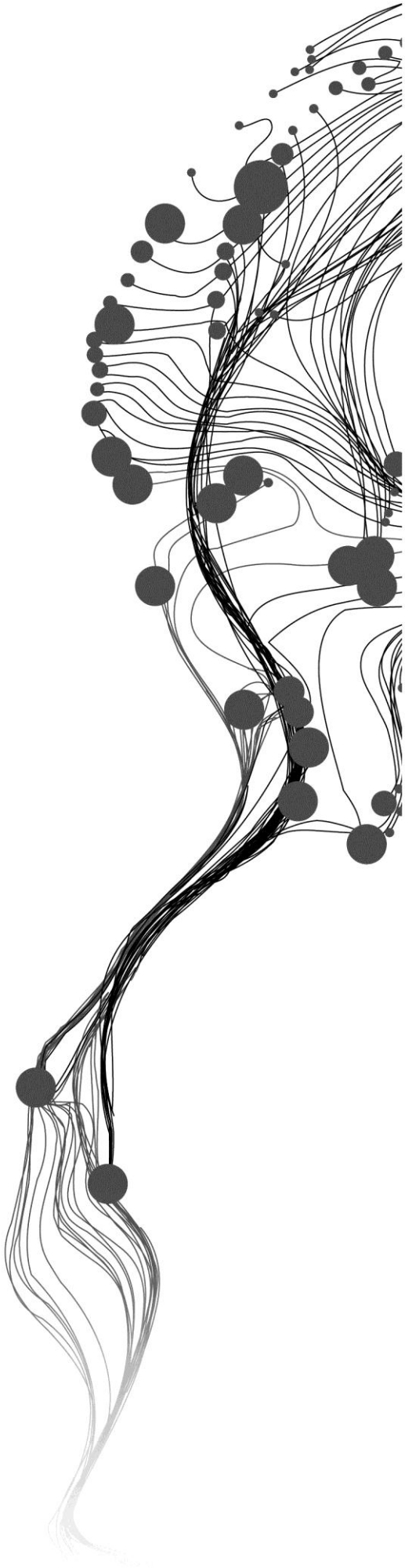

# THE QUALITY OF GLACIER OBSERVATION: THE DEBRIS AREAS AND THEIR ROLE IN SIZE ESTIMATION

MUSLIM MIRZOSHOEVICH, BANDISHOEV
Enschede, The Netherlands, March, 2011

Thesis submitted to the Faculty of Geo-Information Science and Earth Observation of the University of Twente in partial fulfilment of the requirements for the degree of Master of Science in Geo-information Science and Earth Observation.
Specialization: Geoinformatics

SUPERVISORS:
Ms Dr. A. Dilo
Prof. Dr. Ir. A. Stein

THESIS ASSESSMENT BOARD:
Chair: Prof.Dr.Ir. A. Stein
External examiner: Dr.Ir. G.W.A.M. van der Heijden
Supervisor: Ms Dr. A. Dilo
Second supervisor: Prof.Dr.Ir. A. Stein

# ABSTRACT

Glacier mapping from satellite multispectral image data is hampered by debris cover on glacier surfaces. Information on the spatial distribution and spatial-temporal dynamics of debris, however, bears various kinds of uncertainties. Debris exhibits the same spectral properties as lateral and terminal moraines and as bedrock outside the glacier margin. Multispectral classification alone is thus not suitable to properly assess its extent. Therefore, additional information has to be included, like the low slope angles and curvature characteristics.

In this research we proposes a random set method for uncertainty modelling of debris-covered glaciers extracted from remote sensed data. Here, we analyse the Fedchenko glacier situated in the Pamirs mountains. Clean glacier ice and debris cover area broad gradual boundaries are represented by random sets, and their statistical mean and median are estimated. The paper combines the advantages of an automated multispectral classification for clean glacier ice and snow with slope information derived from a digital elevation model (DEM). Random sets are well suited to estimate the boundaries thus obtained.

The paper uses an SRTM3 DEM that is resampled to 30m. From 1999 Landsat ETM+ image the results show that the mean area of clean glacier ice is 841.87 $km^2$, and 94.39 $km^2$ for debris-covered area.

Some geomorphological data has been lost in this process and in order to improve the method outcomes, a finer DEM is required for high-mountain areas. We conclude that method based on random set theory has a potential to serve as a general framework in uncertainty modelling of debris-covered glaciers and is applicable for mountainous glaciers.

Keywords: Random set theory; Uncertainty Spatial data model; Glacier mapping; Debris cover; DEM analysis.

# ACKNOWLEDGEMENTS

I acknowledge and express my special gratitude to my supervisor Dr. Arta Dilo whose scholarly advice, help and continuous encouragement have contributed significantly to the completion of this study. I want to thank her for providing me with constructive critics which has immensely impacted the result of this thesis.

A special thanks to Professor Dr. Alfred Stein for his comments, recommendations and advices that helped me a lot to overcome some academic challenges while completing this study.

Moreover, I am indebted to the course director, lectures and all my fellow students for their invaluable input and for being a great source of support to me during my study. I am grateful to my new friends for creating academic environment while sharing the lab which helped me to complete this research project.

I really appreciate the help of the ITC IT department for installing the required software and helping me in obtaining the satellite images for my research. Also I am appreciative of the services of ITC library staff for making available all the high quality information, including the recommended literatures and other relevant text books during my studies and thesis.

The World Bank Graduate Scholarship Program made possible my study in the Netherlands, which has assisted me to improve my knowledge skills on Geoinformatics. At the same time it was great opportunity to learn and experience the diverse culture and traditions of Dutch people. Therefore, I express my deep gratitude the member of Scholarship Programme for their generosities and kind supports which has played a vital role in both my studying and research project.

Finally, I want to say special thanks for my family members for their love, supports and affection during my studies in the Netherlands. This work would not have happened without theirs advices, courage and support.

Thank you all.

# TABLE OF CONTENTS

# LIST OF FIGURES

# LIST OF TABLES

# 1. INTRODUCTION

## 1.1. MOTIVATION AND PROBLEM STATEMENT

As an integral part of cryosphere mountain glaciers constitute one of the most important components of the Earth's natural system. They are natural integrators of changes in climate and serve as sensitive indicators of climate changes. The problem of glaciers shrinkage around the world is an obvious evidence of global warming (Haeberli et al., 1999). Glaciers are the source of fresh water and cover significant part of many mountain ridges on the earth. For example, in Tajik Pamirs totally 6,730 glaciers with 7,493 km squared were identified in mid of 1970s (Kotlakov et al., 2008) and they constitute the main source of fresh water for most of rivers originating from the region. Therefore, an accurate assessment of snow cover and its changes in time is of vital importance for the planning and management of water resources.

First of all it is important to be clear about what is a glacier? In this research we rely on definition developed within the context of the GLIMS project (Raup, 2010). While this definition is based on other official documents like the UNESCO guidelines, they were adopted for the purpose of satellite-based mapping. The GLIMS definition of a glacier states that: "A glacier or perennial snow mass consists of a body of ice and snow that is observed at the end of the melt season, or, in the case of tropical glaciers, after transient snow melts. This includes, at a minimum, all tributaries and connected feeders that contribute ice to the main glacier, plus all debris-covered part of it. Excluded all exposed ground, including nunitaks" (Racoviteanu, 2008).

Due to the remoteness, vastness and inaccessible nature of the mountain glaciers, remote sensed data are likely the best and the only effective tool for regular mapping of glaciers in a comprehensive and effective manner. Over the years, a number of remote sensing techniques for automated mapping of glacier snow and ice (GSI) by means of multispectral classification are available. Commonly used techniques such as single band ratios (Bayr et al., 1994; Paul, F., Huggel, et al., 2002; Paul, F., Kääb, et al., 2002) and Normalized Difference Snow Index (NDSI) (Dozier, 1989; Hall et al., 1995; Hendriks & Pellikka, 2007; Negi et al., 2009; Silverio & Jaquet, 2005) take advantage of the high brightness of snow and ice in the visible wavelength to separate them from darker areas such as rock, soil or vegetation.

However, the greatest difficulty in glacier mapping from remote sensed data is the presence of debris covered area (DCA) on glaciers (Bolch, T. et al., 2008; Bolch, T. & Kamp, 2006; Kargel et al., 2005; Paul, F. et al., 2004). Glacier areas covered by debris confound the existing techniques. Debris-covered glacier has a similar visible (VIS) and near-infrared (NIR) spectral signature to the surrounding terrain, lateral and terminal moraines – outside of a glacier margins due to similar reflectance at these wavelengths and thus it complicates the mapping of glaciers (Bolch, T. & Buchroithner, 2007). Here, the traditional multi-spectral classification techniques are of limited value because of the difficulties in using multi-spectral data to separate debris-covered glaciers (supraglacial debris) from periglacial debris/moraines. A number of methods have been proposed to address this problem. These methods use the additional information provided by topography (Bishop et al., 2001), neighbourhood analysis (Paul, F., et al., 2004) and thermal radiation (Taschner & Ranzi, 2002b). But, still the existing techniques for mapping of debris-covered

glaciers have limitations in delineation of glaciers boundary where the transition between debris-covered glacier and adjacent terrain is gradual.

Performing spatial analysis, geographic entities need to be extracted from images and represented as crisp or uncertain objects. Most of real-world entities on remote sensing images usually have gradual transition boundary due to either the scale of observation or thematic poor definition (Stein et al., 2009). Therefore, spatial data modelling methodology should be general enough to embrace uncertainties as a representation of real-world objects. Uncertain spatial objects can be modelled by means of fuzzy set theory, which deals with imprecise definitions of concepts by mean of membership functions (Dilo et al., 2007). Since the assignment of the membership function is subjective in nature, a major obstacle of the fuzzy approach is determination of the membership function for a spatial object (Robinson, 2003). To handle the uncertainty in spatial objects random set theory has been viewed as a generalization of uncertainty theory (probability and fuzzy theory) (Mahler, 2007). Some concepts of random set theory are introduced and summarized in the context of geo-information and environmental sciences by (Zhao et al., 2010). Also, random sets are flexible to model dynamic objects in space and time. Therefore it can involve both spatial uncertain objects and spatial-temporal uncertain objects within the same framework (Zhao et al., 2009).

Commonly used image segmentation method to extract GSI from remote sensed data includes thresholding approach. Image rationing and NDSI techniques combine the advantage of automated multispectral classification for clean glacier ice and by thresholding segmentation extract GSI as a crisp object. Both NDSI and band rationing classification techniques have the advantage of being fast and robust, but the main difficulties in automatic mapping of glaciers using band ratios remain due to the presence of debris on glaciers. That is due to similar reflectance of VIS/NIR spectral signature of debris-covered glaciers to the surrounding moraines (Kargel, et al., 2005). Spectral information alone is insufficient for debris-covered glacier mapping. Combining band ratios with topographic information is a promising approach for semi-automated mapping of debris-covered glaciers. For example, (Paul, F., et al., 2004) devised a semi-automatic approach which used ratio (VIS/NIR) image, Intensity Hue Transformation (IHS) and a slope image (<24°) to map a debris-covered glacier in the Swiss Alps. However, this approach fails when transferred to the Himalayan debris-covered glaciers in its original form. The probable reason for its failure in the other areas arises from the fact that the method involves derivation of various thresholds at different stages such, as the band ratios, slopes and hue thresholding, which often tend to be scene-specific (Shukla et al., 2010).

Thresholding only takes the value of the image pixels into account. The selection of the threshold value in the NDSI distribution to distinguish between GSI and non-GSI is a critical task as a slight change can lead to overestimation or underestimation of the areal extent of snow cover. The threshold value may be different for different satellite sensors and for different seasons (Dozier, 1989; Hall, et al., 1995). Since it is arbitrary to choose a single-valued threshold, uncertainties exist in any segmentation results and can have a large effect on the subsequent spatial analysis (Lucieer & Stein, 2002). Thus, it is difficult to precisely choose segmentation parameters and to identify and extract clean glacier ice with vague boundaries from band ratios image, or to extract DCA of a glacier which have gradual transition to the non-glacier surrounding area.

Information on spatial distribution of debris-covered glaciers from remote sensed data bears various kinds of uncertainties. A stochastic method, random sets can be used for modelling of spatial and spatial-temporal uncertainties of natural objects (Zhao, et al., 2010). In order to investigate uncertainties that are inherent to observations of glaciers from satellite imageries, a random set method is proposed in this

research for uncertainty modelling of debris-covered glaciers. A glacier with uncertainties can be treated as a randomly varying set, i.e. a random set. In this research we show that random sets can serve as a framework to model debris-covered glaciers with inherent uncertainties.

## 1.2. RESEARCH IDENTIFICATION

To the best of our knowledge, no research has been done to apply random set theory to uncertainty modelling of debris-covered glaciers. Commonly used image segmentation methods for extracting clean glacier ice (Paul, F., Huggel, et al., 2002) and methods which use additional information such as geo-morphological parameters (Bolch, Tobias, 2007) for extracting debris-covered area of glaciers do not consider the uncertainties inherent to the glaciers. Still, there is no technique for glacier mapping taht can be used to model and quantify the uncertainties. Therefore, in this research a random set method is proposed to model and quantify uncertainty of debris-covered glaciers.

### 1.2.1. RESEARCH OBJECTIVES

The overall objective of this research is to model the uncertainties of debris-covered glaciers in space and time by applying a random set method.
The following are the specific research objectives:

1. To model the spatial uncertainties for a debris-covered glacier;
2. To model the uncertainties of glaciers change in space and time;
3. To estimate the clean glacier ice and debris-covered part of a glacier;
4. To assess suitability of the random set method in delineation of debris-covered glaciers.

### 1.2.2. RESEARCH QUESTIONS

1. How to define a random set for spatial objects?
2. How to implement covering functions for the spatial objects?
3. How to estimate the spatial boundaries of debris-covered glaciers?
4. What is the spatial extent of clean glacier ice and glaciated area covered by debris?
5. What is the variation of debris-covered glaciers in space and time?
6. Does the random set method give better results than crisp classifier methods?

### 1.2.3. INNOVATION AIMED AT

The research innovation is on applying a random set method for uncertainty modelling of debris-covered glaciers and estimation of extensional uncertainty in space and time. In contrast to existing crisp based methods, in this research we use the method allowing us to model and quantify uncertainties inherent to debris-covered glaciers.

### 1.2.4. RELATED WORK

(Zhao, et al., 2010) introduced some concepts of random sets theory in the context of environmental science. The application of the method had been illustrated in uncertainty

modelling for grassland and vegetation identification. Also, the involving of random sets method both in spatial and temporal uncertain objects under a uniform framework is given in (Zhao, et al., 2009).

# 2. LITERATURE REVIEW

## 2.1. APPLICATION OF REMOTE SENSING IN GLACIOLOGY

The spectral property of glaciers governs their separability from other land covers on remotely sensed data. Glaciers must be spectrally discernible from the surrounding, in order to be detected from remotely sensed data. Figure 1 shows the spectral reflection properties of glacier ice, fresh snow and firn in the visible/near infrared (VNIR), short-wave (SWIR) and thermal (TIR) regions of the spectrum. These curves suggest that some properties can be spectrally discriminated as long as the spectral resolution of the image is sufficiently narrow. Although surface albedo of glaciers shows a considerable short-term and spatial variability of objects(Gao & Liu, 2001).

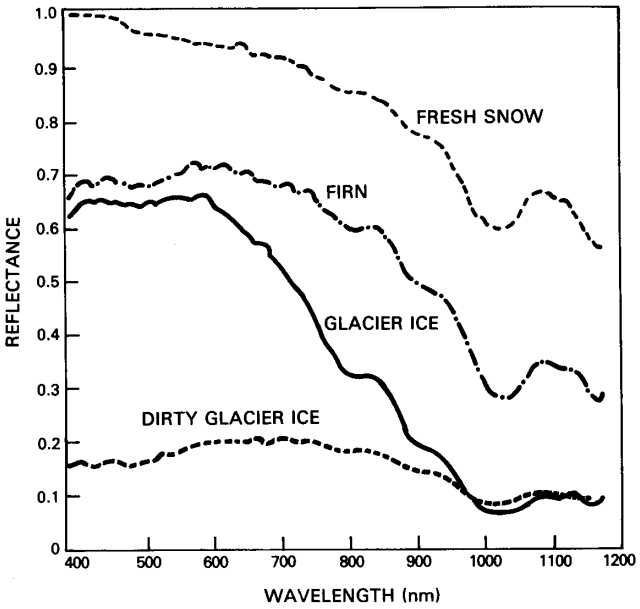


Figure 1. Spectral reflectance curves between for fresh snow, firn, glacier ice and dirty glacier ice.

Numerous remote sensing based studies have been carried out for mapping of glacier and snow cover applying different techniques (Table 1).

Table 1. Summary of glacier outline extraction methods.

| Classification Method | Suitable terrain type |
|---|---|
| Manual digitization (Hall et al., 1992) | Any |
| Spectral band ratio and threshold (Keshri et al., 2009; Paul, P., 2000) | Clean glacier ice and snow |
| Normalized Difference Snow Index (Dozier, 1989; Silverio & Jaquet, 2005) | Clean glacier ice and snow |
| Geomorphometric-based methods (Bolch, T., et al., 2008; Paul, F., et al., 2004) | Debris-covered glaciers |
| Thermal band methods (Taschner & Ranzi, 2002a) | Clean or lightly debris-covered glaciers |

Below are given application of the techniques for mapping of glacier snow and ice and debris-covered area of glacier.

### 2.1.1. METHODS FOR MAPPING OF GLACIER SNOW AND ICE

Multispectral satellite imageries from the Landsat TM and ETM+, SPOT and ASTER sensors have been used for automated clean glacier ice mapping (Bolch, T. & Buchroithner, 2007; Bolch, T. & Kamp, 2006; Kääb et al., 2002). Automatic delineation of clean glacier ice is based on the high reflective of snow and ice in the visible wavelengths (VNIR; 400 – 1200 nm) compared with a very low reflectivity in the shortwave infrared (SWIR; 1400 - 2500 nm) (Dozier, 1989). The most widely used techniques such as TM4/TM5, TM3/TM5 and the normalized difference snow index (NDSI), take advantages of the spectral uniqueness of snow and ice in the SWIR wavelengths (Figure 2.1.) to separate them from non-glaciated area such as rock, vegetation or soil (Hall, et al., 1995; Paul, F., Huggel, et al., 2002).

The most efficient method is based on a thresholded ratio image from the raw digital numbers (DN) of bands TM3 or TM4 and TM5 that utilizes the spectral differences of ice and snow in the shortwave infrared part of the spectrum compared with other surfaces. The method is simple to apply, the threshold value is robust and the results are very accurate for debris-free ice (Albert, 2002; Andreassen et al., 2008). (Andreassen, et al., 2008) applied TM3/TM5 ratio using raw DN with a threshold of 2.0 (TM3/TM5 > 2.0) and yielded satisfactory results for Norwegian glaciers where debris covered ice is sparse. (Paul, F. & Andreassen, 2009) found that for Svartisen region in Norway, a thresholded ratio image where pixels are classified as ice or snow when (TM3/TM5) > 2.6 with raw DN is used. An additional threshold in TM1 (DNs >59) was applied to improve glacier mapping in cast shadow. (Paul, F., Huggel, et al., 2002) applied different glacier mapping methods such as TM3/TM5 versus TM4/TM5 using DN. The TM4/TM5 ration image using the raw DN proved to be the best method with respect to glacier areas in cast shadow (Paul, F., Kääb, et al., 2002).

NDSI is calculated as **(**VNIR- SWIR)/(VNIR+SWIR), where VNIR is band 2 of Landsat TM or ETM+ sensors and SWIR is band 5. The resulting NDSI image has value from -1 to 1 and is segmented using a threshold value to obtain a binary map of glacier – non-glacier areas (Hall, et al., 1995). Pixels with NDSI values greater than the threshold value are assigned to snow/ice class, and those less than the threshold value are classified as non-snow or non-ice. (Dozier, 1989) found that the correct threshold values can be derived theoretically if the atmospheric properties at the time of the satellite overpass are known. However, the threshold can be selected by inspection of images, as the human eye can estimate the correct values by using textural features. In testing snow-covered areas using Landsat TM scenes, NDSI threshold values greater than or equal to approximately 0.4 were found by (Dozier, 1989) to represent snow and glacier. The threshold chosen by (Racoviteanu, A. E. , Williams, et al., 2008) was 0.7 (NDSI > 0.7: snow/ice) for Sikkim glacier in Himalayas, but for Cordillera Blanca the suitable threshold was 0.5 - 0.6 (Racoviteanu, A. E., Arnaud, et al., 2008). The NDSI algorithm correctly classified the clean ice in these two areas, including most of the ice in shadow, and also masked out clouds. For Cordillera Blanca glacier, (Silverio & Jaquet, 2005) found that acceptable NDSI thresholds for two scenes were equal to 0.40 and 0.52. The NDSI technique classification can be used to classify the clean glacier ice, including most of the ice in shadow, and also masked out clouds.

These studies emphasized the need to choose the threshold manually depending on the scene characteristics (e.g. haze, sun position and topography). Both NDSI and single-band ratios (such as TM3/TM5 and TM4/TM5) methods are effective for fast clean glacier ice mapping over large areas. However, all band ratio algorithms fail to identify debris-covered glaciers.

### 2.1.2. METHODS FOR MAPPING OF DEBRIS-COVERED GLACIERS

A major constraint in glaciological studies is the mapping of glaciers covered by debris over the glacier boundary (Whalley & Martin, 1986). Debris may be derived either from above a glacier (supraglacial sources) or from its bed (subglacial sources). Supraglacial sources consist of debris which falls or flows onto surface of the flakier from valley sides or mountains which extends above its surface. Debris may also be deposited on a glacier surface by windfall (dust, volcanic ash, sea salt), avalanches or by human action. Subglacial debris is derived through glacial erosion (Bennett & Glasser, 1996). Due to the fact that debris covers over glaciers and the adjacent periglacial debris lying outside the glacier boundary is derived from valley rock itself, theirs spectral responses are quite similar. The spectral similarity makes delineation of the actual glacier boundary difficult (Bolch, T., et al., 2008; Paul, F., et al., 2004).

Mapping of debris-covered glaciers is important for accurate determination of glacier area and for further applications. Debris-covered glacier area confounds the band ratio techniques, because the spectral signature of debris is similar to that of surrounding terrain. Thus, spectral information alone is insufficient to delineate debris cover. A variety of techniques are available for mapping of debris-covered glaciers. One way to distinguish between a debris-covered glacier and surrounding terrain is by using surface temperatures as supraglacial debris is often cooler due to underlying ice (Lougeay, 1974). (Ranzi et al., 2004) used this idea and found out that the method can be applied for glacier mapping when thickness of debris cover did not exceed 40 to 50 cm (Ranzi, et al., 2004; Taschner & Ranzi, 2002a)(Ranzi, et al., 2004; Taschner & Ranzi, 2002a)(Ranzi, et al., 2004; Taschner & Ranzi, 2002a)(Ranzi, et al., 2004; Taschner & Ranzi, 2002a)(Ranzi, et al., 2004; Taschner & Ranzi, 2002b)(Ranzi, et al., 2004; Taschner & Ranzi, 2002b). An automated morphometry-based approach to outline the debris-covered glaciers of the Mt. Everest area based on ASTER data is presented by (Bolch, T. & Buchroithner, 2007), which used various DEM derived geomorphometric parameters (elevation, slope, curvature, and aspect). Based on these parameters, the model could delineate debris-covered glaciers but major inaccuracies remained in the areas where the lateral moraines were missing or not represented in the DEM. (Paul, F., et al., 2004) developed a semi-automated method for glacier mapping based on slope characteristics, a map of vegetation cover and a TM4/TM5 band ratio. The result highly depends on DEM quality and the type of debris-covered glaciers being mapped. (Bolch, T. & Buchroithner, 2007) used various morphometric approaches in combination with thermal information but the approach has limitation in correctly mapping the glacier boundary in areas where transition between the glacier and adjacent terrain was gradual and the lateral moraines were too small to be represented on DEM.

DEMs offer the most common method for extracting topographic information and enables the modelling of surface process. DEMs play an important tool for the analysis of glaciers and glaciated terrains (Paul, P., 2000). The elevation data are used in glaciology to derive glacier parameters such as length, terminus elevation, median elevation, hypsometric information and glacier flow patterns, and for orthorectification of satellite imagery. Also, changes in glacier surface elevation can be determined by application of time-series DEMs (Racoviteanu, A. E. et al., 2007).

Quality control of the DEMs is essential for glacier studies before they are applied. Acceptable errors depend on the intended application. DEMs can be derived from topographic maps by interpolation either points or contour lines digitized from these maps. The accuracy of the resulting DEM is largely dependent on the type of terrain and interpolation method used (Racoviteanu, A. E., et al., 2007). Various ASTER DEM derived geomorphometric parameters (elevation, slope, curvature, and aspect) were used by (Bolch, T. & Buchroithner, 2007) for the morphometry-based approach for debris-covered glaciers delineation.

The results show the proof of the concept proposed but it was obvious that the resolution of the DEM is not sufficient. (Bolch, T. & Kamp, 2006) generated DEMs from SRTM3 and ASTER and compared with each other and with reference data. Both DEMs are of good use for glacier delineation with Landsat TM4/TM5-ration images, multispectral and morphometric analysis for Bernina Group glacier in the Central Alps. On the other hand the SRTM3 DEM lacks data points at mountain peaks and steep slopes due to the radar shadow effect. However such areas can be substituted by ASTER DEM (Kääb, 2005). The main advantage of ASTER DEMs is the capability to generate multitemporal DEMs which supports glacier monitoring studies. In his research, (Paul, F., et al., 2004) used DEM25 from Swiss Federal Office of Topography with 25 m spatial resolution to derive the slope information for the automated glacier mapping approach. He compared the DEM25 with ASTER derived DEM and concluded that ASTER stereo data may provide useful results for many remote high-mountain regions with poor DEM data.

### 2.1.3. CHALLENGES IN MAPPING OF DEBRIS-COVERED GLACIERS

Currently, there is no single best algorithm for debris-covered glaciers mapping that can be applied to large regions without manual corrections of the resulting outlines (Racoviteanu, A. E. et al., 2009). The challenges in debris-covered glaciers mapping relate to accurate identification of the glacier terminus and delineation of debris-covered area of glaciers from surrounding terrain. The delineation and representation of glaciers with inherently vague extensions is a challenge. Its ignorance or reduction to lines as often occurs on congenital maps may be a simplification, which is not considered the uncertainty. One of the greatest remaining challenges is the validation of existing debris-cover algorithms. As it may be difficult even in the field to locate the boundary of a debris-covered glacier (Haeberli & Epifani, 1986).

## 2.2. UNCERTAINTY MODELING OF SPATIAL OBJECTS

Most of real-world spatial objects, including debris-covered glaciers on remote sensing images usually have transition zones and uncertain boundaries due to the scale of observation or thematic poor definition. Conventional pixel-based approaches generate maps with exclusive categories and do not take uncertainties into account. Therefore, spatial data modelling methodology should be general enough to embrace uncertainties.

A number of soft classification and uncertainty modelling methods have been developed for classifying and representing nature landscapes such as beach (Van de Vlag & Stein, 2007) and grassland (Zhao, et al., 2010). Debris-covered glaciers can be modelled as spatial objects with inherent uncertainties by means of fuzzy set theory, which deals with imprecise definitions by mean of membership functions. A major obstacle of the fuzzy approach is determination of the membership function, since its assignment is subjective in nature (Robinson, 2003).

### 2.2.1. RANDOM SET THEORY

In this research we are interested in analyzing extensional uncertainties of debris-covered glaciers. Before carrying out measurements, we need a spatial data model to describe, interpret and formalize the spatial information.

The possible outcomes of an image segmentation by thresholding are determined in part by random factors forming the space of elementary events (or segmented image regions) $\Omega$. Other events, expressed as qualitative concepts, are formed by combinations of elementary events, i.e., subsets of $\Omega$. These events may thus be organized in a structure of subsets, the δ-algebra on $\Omega$, denoted by $\delta_\Omega$. This structure ensures a predictable behaviour in operations with subsets such as complement, union, intersection etc. Ir also allows us to measure how likely an event is by introducing a probability measure $Pr_\Omega$ in the measurable space $(\Omega, \delta_\Omega)$. The tuple $(\Omega, \delta_\Omega, Pr_\Omega)$ is called a probability space and it summarizes the experiment or process.

For the formal definition of a random variable, let $(\Omega, \delta_\Omega, Pr_\Omega)$ be a probability space and $(\Xi, \delta_\Xi)$ a measurable space. Every $(\delta_\Omega - \delta_\Xi)$-measurable mapping $X: \Omega \rightarrow \Xi$ is called a random variable. A measurable mapping verifies that for all $\mathcal{B} \in \delta_\Xi$ implies $X^{-1}(\mathcal{B}) \in \delta_\Omega$.

$$Pr_X(\mathcal{B}) = Pr_\Omega(X^{-1}(\mathcal{B})) = Pr_\Omega\{\omega: X(\omega) \in \mathcal{B}\}, \ \forall \mathcal{B} \in \Xi$$

The definition of a random set runs in the same way as a random variable, the only difference is that it associates every elementary event $\omega \in \Omega$ with an event of $\mathcal{U}$ which is a set of subsets of Ξ. That is, we associate with each $\omega \in \Omega$ a subset of Ξ. The mapping associates elementary events of $\Omega$ with elements of, so really it is a random variable between the probability space $(\Omega, \delta_\Omega, Pr_\Omega)$ and the measurable space $(\mathcal{U}, \delta u)$.

$$Pr_X(\mathcal{B}) = Pr_\Omega(X^{-1}(\mathcal{B})) = Pr_\Omega\{\omega: X(\omega) \in \mathcal{B}\}, \forall \mathcal{B} \in \delta u$$

This means that a random set is a multi-valued mapping between the spaces $\Omega$ and Ξ as shown in Figure 2.

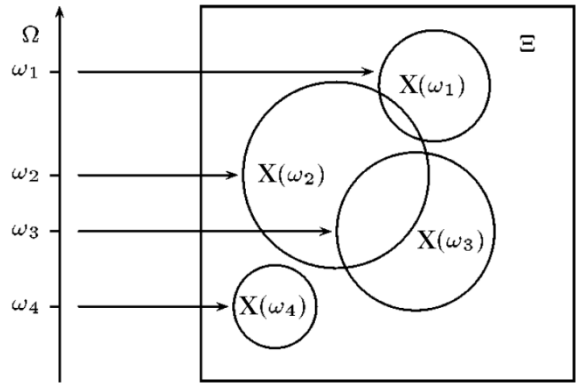


Figure 2. A random set as multivalued mapping from $\Omega$ to Ξ (Nunez-Garcia & Wolkenhauer, 2002)

Note that a random set can be seen as a random variable from $\Omega$ to $\mathcal{U}$ or as a multivalued mapping from $\Omega$ to Ξ since $X(\omega) \in \mathcal{U} \Rightarrow X(\omega) \subseteq \Xi$. The probability space is the mathematical model that is used to represent and explain the experiment.

Let us to denote the space of an image as $I \subset \mathbb{R}^2$ in Euclidian space, where the pixel $\xi$ is a basic element. The measure space that carries random objects is denoted by $\mathcal{U}$ , being a set of subsets of $\mathbb{R}^2$, i.e. $\mathcal{U} \subseteq \mathcal{P}(\mathbb{R}^2)$. For uncertainties modelling of the spatial objects by a random set method random region objects are defined: (1) random point/variable, and (2) random region.

A random region is defined as a random set Γ on a space $\mathcal{U}$ that contains a finite collection of random points. Random set can also be presented by focal elements $\mathcal{A}_i$: i={1,2,...,n} with corresponding

uncertainty assignments, denoted as a collection of pairs $\{\mathcal{A}_i\ m_i\}$ (Figure 3). The focal elements are regions which are subsets of $\mathbb{R}^2$: $\mathcal{A}_i \in \mathcal{P}(\mathbb{R}^2)$. If a random set consists of n focal elements with equal probability, then $m_i = \frac{1}{n}$.

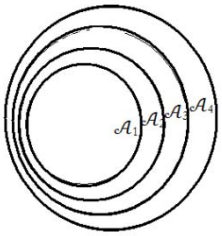


Figure 3. Focal elements of a random set.

A random set Γ in Euclidian space $\mathbb{R}^2$ associate a function $Pr_\Gamma$: $\mathbb{R}^2 \rightarrow [0, 1]$ to every $\xi \in \mathbb{R}^2$. This function is called the covering function. The covering function of a random set can be estimated from its focal elements $\mathcal{A}_i$, i={1,2,...,n} by:

$$Pr_\Gamma(\xi) = \frac{1}{n}\sum_{i=1}^{n} I_{\mathcal{A}_i}(\xi)\ ,\ \xi \in \mathbb{R}^2,\ \mathcal{A}_i \in \mathcal{P}(\mathbb{R}^2) \quad (1)$$

where $I_{\mathcal{A}_i}$ is the indicator function of $\mathcal{A}_i$: i={1,2, . . . ,n}:

$$I_{\mathcal{A}_i} = \begin{cases} 1, & \xi \in \mathcal{A}_i \\ 0, & \xi \notin \mathcal{A}_i \end{cases}$$

The covering function can be interpreted as the probability of an element $\xi \in \mathbb{R}^2$ being covered by a random set (Figure 4).

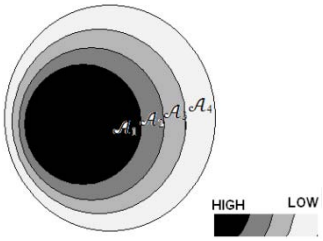


Figure 4. Probability estimation by covering function.

The set $\Gamma_p = \{\xi \in \mathbb{R}^2,\ 0 \leq p \leq 1: Pr_\Gamma(\xi) \geq p\}$ is called a p-level set.
Special cases are:

- $\Gamma_s = \{\xi \in \mathbb{R}^2: Pr_\Gamma(\xi) > 0\}$, i.e. the support set, describing the possible part of Γ,
- $\Gamma_{0.5} = \{\xi \in \mathbb{R}^2: Pr_\Gamma(\xi) \geq 0.5\}$, i.e. the median set, describing the 0.5-level set, and
- $\Gamma_c = \{\xi \in \mathbb{R}^2: Pr_\Gamma(\xi) = 1\}$, i.e. the core set, describing the certain part of Γ (Figure 5).

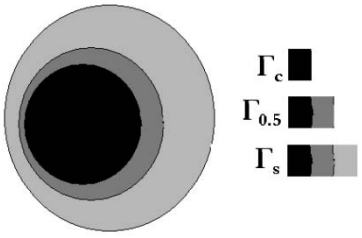


Figure 5. Support, median and core set of a random set.

For example, applying different thresholds for extraction of GSI from an NDSI image may result in n different polygons, denoted as $\mathcal{A}_1, \mathcal{A}_2, \ldots, \mathcal{A}_n$, being samples as well as focal elements of the random region. Figure 6 illustrates a simple example for covering function estimation. $\mathcal{A}_1, \mathcal{A}_2, \mathcal{A}_3, \mathcal{A}_4$ are four focal elements of a random set in $\mathbb{R}^2$ with equal uncertainty assignments i.e. $m_1 = m_2 = m_3 = m_4$, reflected by the equal intervals in y-axis. $\xi_1, \xi_2, \ldots, \xi_7$ are seven elements in $\mathbb{R}$, which are covered by some $\mathcal{A}_i$. The values of the covering function at these points derived by Eq. 1 are shown in the Figure 7.

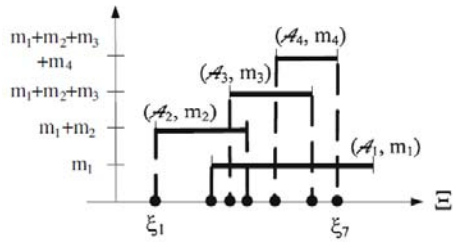


Figure 6. Four focal elements with equal uncertainty assignments construct a realisation of a random set (Zhao, et al., 2010).

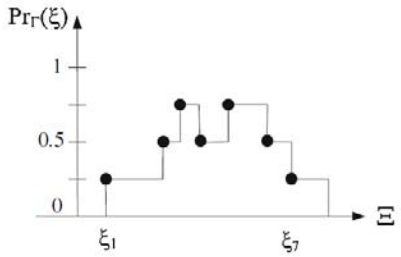


Figure 7. Covering function of the random set estimated by focal elements (Zhao, et al., 2010).

The mean area (EA) of the random region Γ is determined by $EA(\Gamma)=\int_{\mathbb{R}^2} \mathrm{Pr}_\Gamma(\xi)\, d\xi$ (Zhao, et al., 2010). According to the definition of Vorob'ev expectation, the median set of Γ is the 0.5-level set. The mean set, denoted by $\Gamma_m$ is defined as:

$$\Gamma_m=\{\xi \in \mathbb{R}^2, 0\leq p_m\leq 1: \mathrm{Pr}_\Gamma(\xi)\geq p_m\} \quad (2)$$

where $p_m$ is determined such that the set $\Gamma_m$ has the area EA(Γ). If $p_m$ is not unique then one could take the infimum of all such $p_m$s. When $p_m$=0.5, the mean and median are identical. In summary, the Vorob'ev mean of random set is estimated by first determining the mean area $EA(\Gamma)=\int_{\mathbb{R}^2} \mathrm{Pr}_\Gamma(\xi)\mathrm{d}\xi$ and then finding a $p_m$-level set which has area equal to EA(Γ).

The corresponding set-theoretic variance of a random set is defined as:

$$\Gamma_{var}(\xi) = E(I_{\mathcal{A}_i}(\xi)- \mathrm{Pr}_\Gamma(\xi))^2 \quad (3)$$

The sum of $\Gamma_{var}$, denoted as SD and defined as: $SD=\int_{\mathbb{R}^2} \Gamma_{\mathrm{var}}(\xi)\, d\xi$.

The coefficient of variation (CV) is used as a normalized and dimensionless measure:

$$CV=\frac{\int_{\mathbb{R}^2} \Gamma_{\mathrm{var}}(\xi) d\xi}{\int_{\mathbb{R}^2} \mathrm{Pr}_\Gamma(\xi) d\xi} \quad (4)$$

The CV summarizes the dispersion of the distribution of a random set and allowing us to make comparison with other objects. A high CV indicates a larger proportion of objects with a high $\Gamma_{var}$ and thus points to a large extensional uncertainty.

# 3. DATA AND METHODS

Following is the thesis workflow (Figure 8.) and in brief the description of the proposed method which will be considered in the implementation:

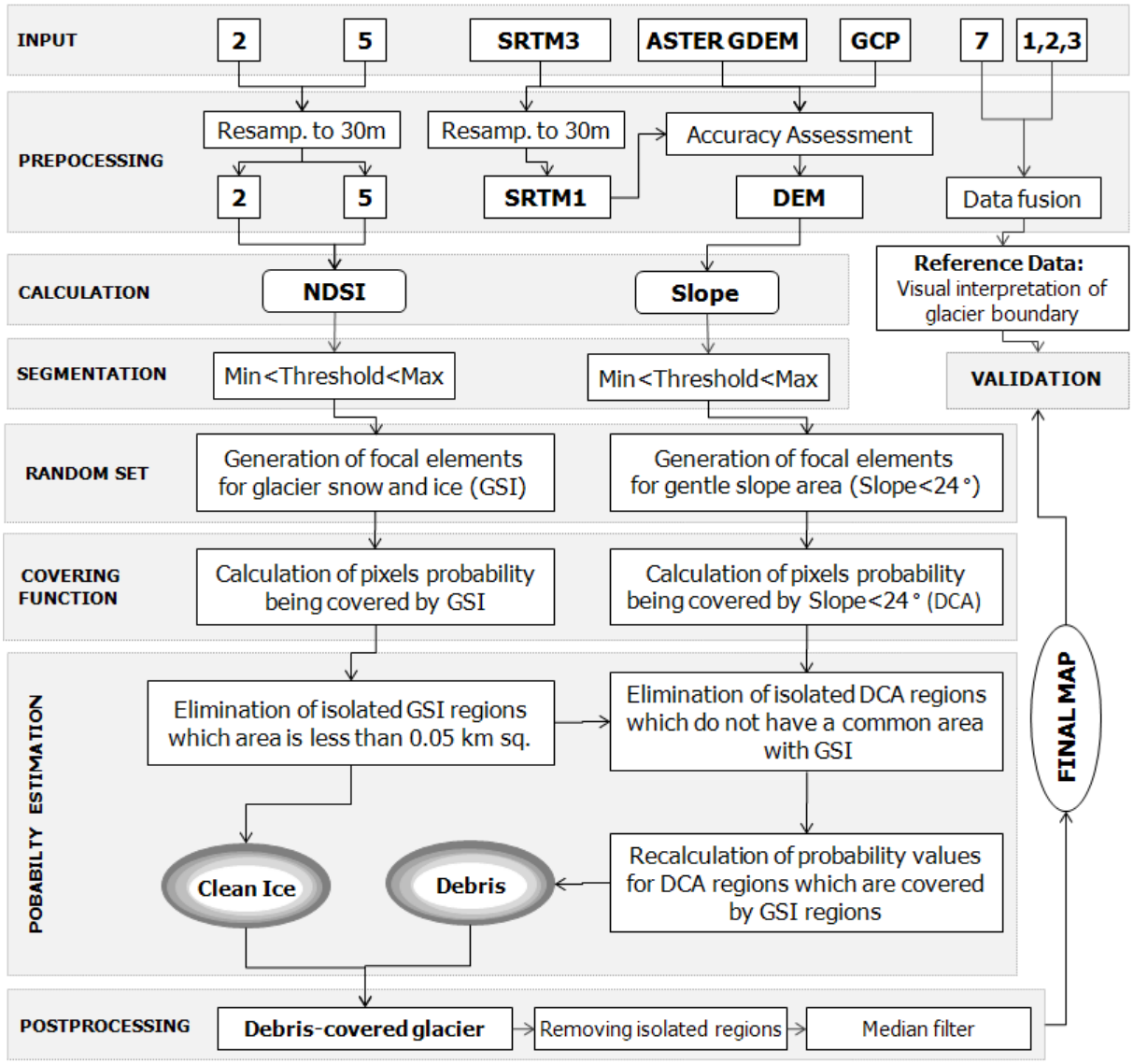


Figure 8. Adopted workflow.

**Datasets selection and pre-processing of datasets:** For glacier observation, it is important that the remotely sensed data is acquired at the end of ablation period and have no significant cloud cover over glaciated area. The proposed approach will be applied with Landsat TM and ETM+ imagery and SRTM3 DEM or/and ASTER GDEM. First of all, the study area will be extracted from the datasets by delineating of a watershed where the study glacier is located. The SRTM3 DEM will be re-sampled to 30 m (SRTM1) by cubic convolution algorithm in order to increase the spatial resolution allowing us to perform morphological operation to detect lateral and terminus moraine on glacier body. The accuracy of DEMs will be assessed against ground control points (GCP) derived from Russian topographic maps. Further, from the most accurate DEM, the slope information will be derived for morphometric analysis of the

glacier. The Landsat images bands will be composited and further pan-sharpened for extraction of validation data by manually digitization.

**Image classification and generation of random sets**: An NDSI image will be utilized for identification of glacier snow and ice (GSI). For identification of debris-covered areas (DCA) of a glacier the slope information will be used, which will be derived from the re-sampled SRTM1 DEM. The thresholding method will be used for GSI mapping from NDSI image and for debris-covered area of a glacier the slope information will be used. The extent of GSI and DCA could vary under different choices of the threshold value. Taking uncertainty into account, the spatial extent of GSI and DCA will be modelled as a random set by a collection of polygons or focal elements extracted by thresholding approach. Thus, in the proposed method we will define threshold ranges for NDSI, and slope images to take into account transition zones. An extent of ranges for both images will be defined and the number of total threshold value will be obtained to slice NDSI and slope images and make samples of binary images (GSI – non-GSI, DCA– non DCA). Each sample will be a realization of a focal element of random sets.

**An implementation of covering functions:** The covering function of a random set can be interpreted as the probability of a pixel being covered by a random set and it will be used for estimation of an image pixels probability being a part of GSI or DCA.

**Identification of debris-covered area of glaciers:** By intersection of two derived random sets: GSI and DCA, the final map of a glacier covered by debris will be obtained. Below are given rules of classification in Table 2.

Table 2. Defined rules for identification of debris-covered glaciers.

| IMAGES | RESULTS | | |
|---|---|---|---|
| Slope<24 | No | Yes | Yes/No |
| GSI | No | No | Yes |
| **CLASSIFICATION** | **Other** | **DCA** | **GSI** |

**Glacier area estimation:** To estimate the images objects area the mean area of the random sets will be used. The area of the random set can be estimated by integration of image pixels which probability greater than 0.

**Temporal analysis:** Times series data analysis will be performed for identification and classification of GSI and DCA from temporal images. The uncertain area of both objects will be identified and quantified and will compared to the other temporal images..

**Validation:** Comparison of the proposed algorithm results with the reference data will be performed to test the accuracy of the research method for uncertainty measurement.

## 3.1. STUDY AREA

The study case for this research is situated in the western part of the Pamirs, Tajikistan (Figure 9). The Pamirs is high-mountain region, in the north-western part of the Central Asian uplands. The western part of this region is a system of ranges, with predominantly latitudinal extension and narrow valleys. In the central part, these ranges are aligned with the meridian range. The major part of the glaciated area is concentrated in the north-western Pamirs, in the middle section of the Zaalaysky range, and in the junction of the Academy of Science range with the system of ranges with latitudinal extension. In the mid of 1970s, 6,730 glaciers (7,493 km² total area) were identified in the Pamirs. The study case of this research is the Fedchenko glacier which is the largest and deepest alpine glacier of Eurasia, 77 km long with an area of almost 650 km² together with its tributaries (Kotlakov, et al., 2008): Bivachny, which is the longest tributary glacier (27 km long), joining at 10 km upstream from the glacier front (Iwata, 2009); Nalivkina; Akademiy Nauk; Eleny Rozmirovicha; Kashalyak.

The southern end of the glacier basin is located at 38º30'16''N, 72º17'00''E; the northern end is 39º05'10''N, 72º18'52''E. The glacier follows a generally northward direction. It begins at an elevation of 6,300 metres above sea level, and eventually melts and empties into the Balandkiik River at an elevation of 2,900 metres (Aizen & Mayewski, 2009). Its waters eventually feed down the Muksu, Surkhob, Vakhsh, and Amu Darya rivers into the Aral Sea.

In view of inaccessible nature of the mountain glaciers and due to the high concentration of glaciers in the Pamirs region, remote sensed data is one of the effective tools for glaciers monitoring in comprehensive and cost effective manner. Especially for the case study area, there is a favourable weather condition (many cloud-free days) for glaciers study (Kotlakov, et al., 2008), which is very important for space imagery.

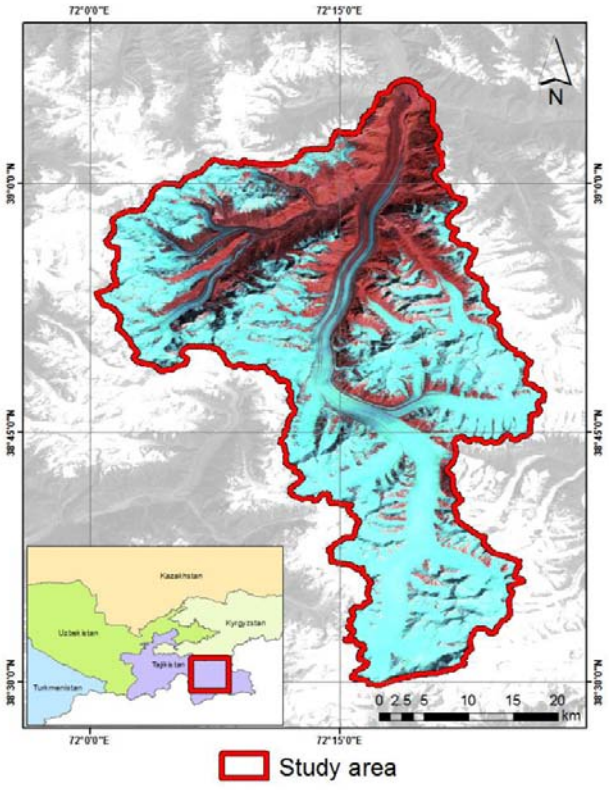


Figure 9. The study area: Fedchenko glacier.

## 3.2. DATA SOURCES AND PRE-PROCESSING

### 3.2.1. DATA SOURCES

The Landsat Thematic Mapper (TM) and Enhanced Thematic Mapper (ETM+) sensors have proven to be a particularly efficient tool for mapping glacier extent and monitoring changes even for small alpine glaciers (e.g. Paul et al., 2002; Kaab et al., 2002). For this research the Landsat images from TM and ETM+ sensors are used due to theirs availability, moderate spatial, spectral and temporal resolution..

For glaciers observations it is important to work with the imagery which have no cloud over the glaciated area and had been taken at the end of the ablation season when the temporary snow cover is at its minimum and all the glacier zones can be clearly demarcated. These factors restrict the use of most available imagery. In total three orthorectified Landsat TM and ETM+ imagery downloaded from USGS web-site (http://glovis.usgs.gov/) are used in this research

The imagery is pre-processed as L1T product Level. The L1T correction process utilizes both ground control points DEM to attain absolute geodetic accuracy. The WGS84 ellipsoid is employed as the Earth model for the Universal Transverse Mercator (UTM) coordinate transformation. Associated with the UTM projection is a unique set of projection parameters that flow from the USGS General Cartographic Transformation Package. The end result is a geometrically rectified product free from distortions related to the sensor (e.g. jitter, view angle effects), satellite (e.g. attitude deviations from nominal), and Earth (e.g. rotation, curvature, relief). The Cubic Convolution method is applied for images resampling and the images are projected to UTM (WGS84 datum) (Masek, 2010). The Landsat 5 and 7 missions have a sun synchronous orbit, produce imagery 185 km wide and have a repeat coverage of 16 days. The images characteristics are given in Table 3.

Table 3. Overview of the Landsat (TM and ETM+) imageries used in this research.

| Date | Sensor | Mission | Sun Azimuth (º) | Sun Elevation(º) | Cloud Coverage(%) |
|---|---|---|---|---|---|
| 27.09.1992 | TM | Landsat 5 | 141 | 42 | 0.00 |
| 07.09.1999 | ETM+ | Landsat 7 | 143.55 | 51.93 | 0.34 |
| 10.09.2009 | TM | Landsat 5 | 143.87 | 50.52 | 3.25 |

The specification of TM and ETM+ images bands are given in Table 4.

Table 4. Landsat TM and ETM+ spectral bands.

| Band | Wavelength (μm) | Part of Spectrum | Spatial Resolution (m) |
|---|---|---|---|
| | TM/ETM+ | | TM/ETM+ |
| 1 | 0.45 - 0.515 | Blue | 30 |
| 2 | 0.525 - 0.605 | Green | 30 |
| 3 | 0.63 - 0.69 | Red | 30 |
| 4 | 0.75 - 0.90 | NIR | 30 |
| 5 | 1.55 - 1.75 | SWIR | 30 |
| 6 | 10.40 - 12.5 | TIR | 120 / 60 |
| 7 | 2.09 - 2.35 | SWIR | 30 |
| 8 | - / 0.52 - 0.90 | Pan | - / 15 |

The Shuttle Radar Topography Mission (SRTM) acquired data in February 2000, from which digital elevation model are created. The elevation data of three-arc seconds (~ 90 meters) is accessible for free over the Internet (http://seamless.usgs.gov/). The data are projected to the UTM projections and elevations are in meters, referenced to the EGS84/EGM96 geoid. The mission report quotes a DEM resolution of several tens of meters, an absolute vertical accuracy of ±6 m (linear error at 90% confidence level, LE90), a relative vertical accuracy of ±6 m (LE90), and a horizontal positional accuracy of about ±20 m (circular error, CE90) (Rabus et al., 2003).

The Advanced Spaceborne Thermal Emission and Reflection Radiometer (ASTER) Global Digital Elevation Model (GDEM) was developed jointly by the Ministry of Economy, Trade, and Industry (METI) of Japan and the United States National Aeronautics and Space Administration (NASA). The methodology used to produce the ASTER GDEM involved stacking all scene-based DEMs, removing residual bad values and outliers, averaging selected data to create final pixel values, and then correcting residual anomalies. It is packaged in 1° by 1° tiles, and covers land surface between 83°N and 83°S with estimated accuracies of 20 meters at 95 % confidence for vertical data and 30 meters at 95 % confidence for horizontal data. (Team, 2009).

### 3.2.2. RE-SAMPLING OF LANDSAT IMAGES

Before different datasets could be used, a few pre-processing steps had to be made. All the spatial and spectral analyses were carried out in ArcGIS and Erdas Imagine. Spatial resolution of the datasets used in this research need to be resampled, if it differs from 30 m. That is because of performing pixel based calculation throughout the research implementation. Landsat TM and ETM+ bands spatial resolution is varying around 30 m and thus need to be resampled. The nearest neighbour method is used for resampling due to less variation in resolution differences. The UTM WGS84 projection (North Zone 43) was used for reprojection.

### 3.2.3. DEM INTERPOLATION AND QUALITY ASSESSMENT

DEM is used to derive the slope information needed for identification of debris-covered area (DCA) of a glacier. In order to map the DCA in details the availability of high spatial resolution of DEM is very important (Paul, F., et al., 2004). For the research area the only available DEM were SRTM3 DEM and ASTER GDEM. Cubic convolution method of interpolation is used to resample SRTM3 to 30 m resolution DEM - SRTM1. The result of interpolation is promised to be sufficient good as it was shown by (Keeratikasikorn & Trisirisatayawong, 2008).

It is necessary to assess the accuracy of interpolated DEM prior to their use, thus the quality assessment is needed. The assessment is performed by comparison of DEMs against reference height data. Absolute vertical accuracies of DEMs were measured by comparison with ground control points (GCP) – elevation points extracted from Russian Topographic Maps (published data: 1979) distributed throughout the study are. Overall, 70 GCP were used as a reference vertical data. The vertical datum of GCP transformed from Pulkovo 42 to WGS84 as SRTM DEMs and ASTEG GDEM are in that datum.

First of all the vertical datum should be the same for all DEMs and GCP. The vertical datum of GCP was transformed from Pulkovo 1942 (Krassovsky spheroid) to WGS84 as both DEMs were based in this

datum. Then subtraction method of comparison was applied to define the most accurate DEM for application in this research.

### 3.3. CALCULATION OF NDSI, NDVI AND SLOPE GENERATION

**GSI identification:** GSI typically has high reflectance in the visible and near infrared region of the spectrum. The GSI characteristics of high reflectance in the visible and low reflectance in the infrared can be used in combination to distinguish GSI from many other spatial features on satellite images. NDSI is calculated as NDSI=(VNIR- SWIR)/(VNIR+SWIR), where VNIR is band 2 and SWIR is band 5 of TM or ETM+ sensors (Figure 10. a and b).

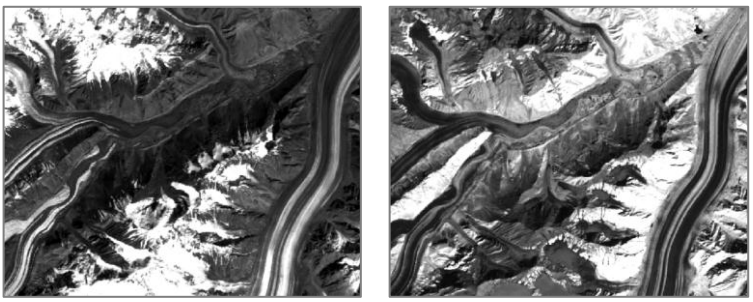

(a) (b)

Figure 10. (a) Band 2 and (b) band 5 of Landsat ETM+ sensor.

**Water body identification:** Water body occurring on the glacier surface or near it cannot be differentiated from an NDSI image along with ice and snow, thus here we apply the Normalized Difference Vegetation Index. To generate an NDVI image Landsat bands 3 (VIS) and 4 (NIR) are used. The formula is the follow: NDVI=(NIR - VIS)/(NIR + VIS).

**DCA identification:** Debris-covered glaciers surface have gentle slope and at the contact of the glacier with the surroundings or bedrock, a distinct change in slope can be observed (Figure 11), which can be utilized for a delineation of debris-covered glaciers (Paul, F., et al., 2004). In this research we will use this idea for identification of DCA.

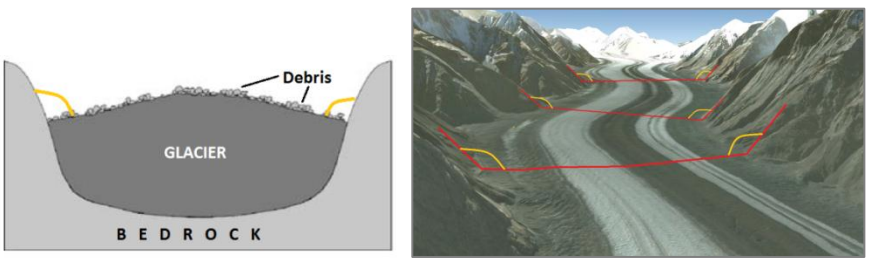


(a) (b)

Figure 11. (a) The gentle slope of a glacier surface can be seen: adopted from (Paul, et al., 2004), (b) Google mage

Slope can be extracted from DEM. Every cell in the output raster has a slope value. The lower the slope value, the flatter the terrain; the higher the slope value, the steeper the terrain. The output slope raster is calculated in as degrees.

## 3.4. IMAGE SEGMENTATION

Thresholding approach of image segmentation is applied to generate random sets. The idea of random set generation is that the extents of NDSI and slope images are sensitive to the different thresholds. Therefore by slightly changing a threshold, we generate a set of objects and construct focal elements of a random set.

To map a debris-covered glacier we use NDSI and slope images. From an NDSI image GSI, and from slope image DCA objects are going to be extracted. To start the extraction of the objects we need to be clear on a range of thresholds we are going to use for segmentation and generation of focal elements for random sets.

**NSDI image segmentation:** For the extraction of GSI the NDSI image is used. The resulting NDSI image has value from -1 to 1 and is segmented using a threshold value to obtain a binary image of GSI – non GSI. Pixels with NDSI values greater than the threshold value are assigned to GSI class, and those less than the threshold value are classified as non-GSI.

The threshold can be selected by inspection of images, as the human eye can estimate the correct values by using textural features. Let us to define the threshold range as $[t_1, t_2]$, where *t1* is the minimum and *t2* is the maximum value for thresholds. This range can be divided into n equal intervals and n+1 thresholds are obtained to slice NDSI images and make samples of binary images. Each sample will be a realisation of a focal element $\mathcal{A}_i$, $i = \{1, 2, \ldots, n\}$ of a random set $\mathcal{A}$. We have no emphasis on thresholds; focal elements have equal probability assignments.

**Slope image segmentation:** Glaciers surface is relatively gentle and at the contact with the surroundings the slope increases. Thus, the slope/steepness information can be used for identification of debris covered part of a glacier (Paul, F., et al., 2004). The idea is to segment plain areas where potentially a glacier might be situated. The minimum threshold value $t_1$ will be identified from mean of slope value from cross-profiles to glacier body. The maximum threshold value is chosen as 24°, which was proven to be efficiently for identification of steep areas where the glacier might be by (Paul, F., et al., 2004). The threshold range $[t_1, 24]$ will be divided into m equal intervals and m+1 thresholds obtained to slice the slope images and make samples of binary images. Each sample will be realisation of a focal element $\mathcal{B}_j$, $j = \{1, 2, \ldots, m\}$, of a random set $\mathcal{B}$. The focal elements have equal probability assignments.

## 3.5. RANDOM SET GENERATION

In this section we discuss the calculation of covering function for GSI and DCA, random sets $\mathcal{A}$ and $\mathcal{B}$ which have been generated by thresholding of NDSI and slope images (see the previous section) and measure the probability of an image pixels being covered by GSI and DCA.

### 3.5.1. COVERING FUNCTION CALCULATION

The covering function can be interpreted as the probability of an image pixel covered by the random set. Suppose, $\xi$ is an image pixel and $\mathcal{A}_i$, $i = \{1,2, \ldots, n\}$ and $\mathcal{B}_j$, $j = \{1,2, \ldots, m\}$ are focal elements of random sets $\mathcal{A}$ and $\mathcal{B}$ generated from NDSI and slope images, accordingly. Then, the probability of an image pixel $\xi$ covered by random regions $\mathcal{A}$ and $\mathcal{B}$ is calculated by,

$$\mathrm{Pr}_{\Gamma}(\xi) = \frac{1}{\mathrm{n}}\sum_{i=1}^{n}\left(I_{\mathcal{A}_i}(\xi)\right)$$

$$\mathrm{Pr}_{\Pi}(\xi) = \frac{1}{\mathrm{m}}\sum_{j=1}^{m}\left(I_{\mathcal{B}_j}(\xi)\right)$$

where $I_{\mathcal{A}_i}$and $I_{\mathcal{B}_j}$ are indicator functions of $\mathcal{A}_i$: $i$ ={1,2, . . . ,n}, and $\mathcal{B}_j$ : j ={1,2, . . . ,m} accordingly.

The covering function returns values in the range of [0, 1]. For pixels which are covered by all focal elements of a random set the function returns 1, and for pixels covered by half of focal elements it returns 0.5. The return value decreases when pixels are covered by less focal elements.

### 3.5.2. GENERATION OF RANDOM SET FOR GSI

GSI on glacier surface does not consist of one connected region but of different detached GSI regions. Some of GSI regions are quite small in size and should not be considered as a part of the glacier as in fact they might not be permanent ice.

Assume that $\Gamma_s=\{\xi \in \mathbb{R}^2: \mathrm{Pr}_{\Gamma}(\xi)\geq 0\}$, is the support set of GSI, describing the possible part of Γ. And $\Gamma_j$, j=1,...,*N* (*N*-total number of detached GSI regions) are support sets of detached GSI components which make up together the whole GSI area, so the random set Γ can be formulated as $\Gamma_s = \bigcup_{j=1}^{N} \Gamma_j$. We eliminate those areas which size is less than 0.05 km². The mean area EA of the random set Γ is determined as $\mathrm{EA}(\Gamma)=\int_{\mathbb{R}^2} \mathrm{Pr}_{\Gamma}(\xi)d\xi$. Thus, we will exclude the GSIs regions which meet the below condition:

$$\mathrm{EA}(\Gamma_j)=\int_{\mathbb{R}^2} \mathrm{Pr}_{\Gamma j}(\xi)\, d\xi < 0.05, \quad \text{for all } \Gamma_j,\ j=1,...,N.$$

### 3.5.3. GENERATION OF RANDOM SET FOR DCA

The debris is transported by the general down slope movement of a glacier towards the terminus and is deposited in the glacier forefield. If local surface slope is too high, debris usually slides farther down until a more gentle slope allows accumulation. Due to a rough mountainous terrain the random set generation for DCA: Π of a glacier requires additional analysis. Thus, we will follow the below steps:

1) The plain areas (0°- d°, d<24°) which make up focal elements for the random set $\mathcal{B}$ occur everywhere in the study area. Thus, first of all it is necessary to eliminate those areas which are not a part of the glacier. One way to distinguish between them is to use the idea that the plain area which is connected to GSI is actually the extension of it and is covered by debris. Thus, for the random set Π some areas have to be eliminated. Let us generate a random set $\Pi_s=\{\xi \in \mathbb{R}^2: \mathrm{Pr}_{\Gamma}(\xi)\geq 0\}$, describing the possible part of Π (DCA), which consists of detached components $\Pi_s=\bigcup_{j=1}^{N} \Pi_j$, and excluding those areas which are not connected to GSI: $\Gamma_s \cap \Pi_j= \emptyset$. The resulting random set will be the following:

   $\Pi_s=\{\xi \in \mathbb{R}^2: \mathrm{Pr}_{\Gamma}(\xi)\geq 0\}$ where $\Pi_s=\bigcup_{j=1}^{N} \Pi_j$ and $\Gamma_s \cap \Pi_j= \emptyset$.

2) Glaciers including its DCA move, or flow, downhill due to the internal deformation of ice and gravity (Bennett & Glasser, 1996). Thus its body is continuous; there should be no gaps in its

body. Lateral moraines on glaciers body indicate the lateral part of glaciers in both sides (Bennett & Glasser, 1996). The moraines will be identified as a part of glacier covered by debris. Due to moraines steepness, theirs probability of being a part of glacier decrease. Plain areas occur beyond lateral moraines will be assigned with higher probability due of having less steepness, which in some cases exceeds 0.5 (Figure 12). But in fact this type of areas should be assigned with low probability of being a debris-covered area because of its disconnection from the main body of glacier by lateral moraines.

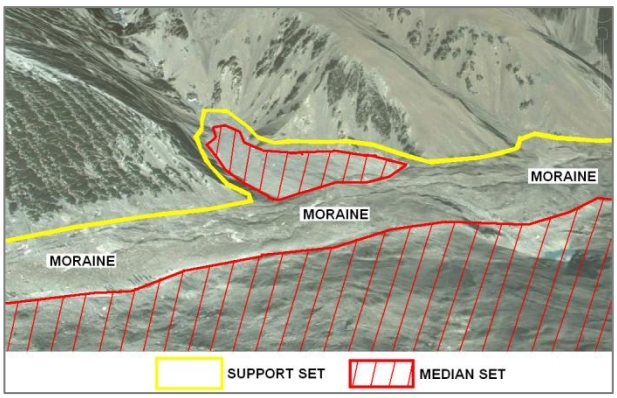


Figure 12. Detached DCA regions

Therefore we conclude that when using the 0.5-level set of $\Pi$: $\Pi_{0.5} = \{\xi \in \mathbb{R}^2: \Pr_{\Pi}(\xi) \geq 0.5\}$, where $\Pi_{0.5} = \bigcup_{j=1}^{N} \Pi_{j(0.5)}$, some regions get detached from each other. That might be the evidence of having of two separate debris-covered glaciers, if both regions are connected to GSI. But if the detached regions are not connected to GSI: $\Gamma_s \cap \Pi_{j(0.5)} = \emptyset$, than it means that the probability of these regions being a part of DCA will be low. Thus, we will re-calculate the probability value for such regions, if $\Pr_{\Pi_{j(0.5)}}(\xi)>0.5$. In this case, we assign the probability value to $\Pr_{\Pi_{j(0.5)}}(\xi)>0.5=0.25$. We will not exclude these regions from our calculation, as there still a low probability of such regions to be a part of DCA, due to theirs low steepness and closeness to the glacier moraines. We re-write the above mentioned:

$$\Pr_{\Pi_{j(0.5)}}(\xi)=0.25, \text{ if } \Gamma_s \cap \Pi_{j(0.5)} = \emptyset \text{ and } \Pr_{\Pi_{j(0.5)}}(\xi)>0.5$$

$$\text{where } \Pi_{j(0.5)} = \{\xi \in \mathbb{R}^2: \Pr_{\Pi_{j(0.5)}}(\xi)>0.5\}.$$

3) The next step is recalculation of elements probability for the random set $\Pi$ (DCA), which elements are covered in the same time by both random sets $\mathcal{A}$ and $\mathcal{B}$. In other words, the probability of a pixel being covered by DCA depends whether a pixel has been classified GSI or not. GSI area of glaciers occurs in plain areas along with DCA. And if the same plain area is covered by GSI than it excludes the presence of DCA. Thus, we need to recalculate, to reduce pixels probability value being covered by DCA, as it is obvious that there is no DCA on a plain area but GSI. So we conclude that, if the probability of an image pixel being covered by GSI and DCA is greater than 0: $\Pr_{\Gamma}(\xi)>0$ and $\Pr_{\Pi}(\xi)>0$, than there is a need of pixels probability recalculation for the random set $\Pi$ by applying $\Pr_{\Pi}(\xi)=1 - \Pr_{\Gamma}(\xi)$.

$$\Pr_{\Pi}(\xi)=1 - \Pr_{\Gamma}(\xi), \text{ if } \Pr_{\Gamma}(\xi)>0 \text{ and } \Pr_{\Pi}(\xi)>0.$$

## 3.6. STATISTICAL PARAMETERS OF RANDOM SETS

The level sets are used to reflect the spatial distribution of the varying sizes of the random sets to quantify the extensional uncertainty of segmented objects. The mean area EA of random sets: Γ (GSI) and Π (DCA) can be determined by.

$$EA(\Gamma) = pixel\ size * \sum_{\xi \in I} \Pr_{\Gamma}(\xi)$$

$$EA(\Pi) = pixel\ size * \sum_{\xi \in I} \Pr_{\Pi}(\xi)$$

where, $\xi$ is a pixel of an image $I$ in Euclidian space $\mathbb{R}^2$: $\xi \in I \subset \mathbb{R}^2$, and $pixel\ size$ – an image pixel size in $km^2$.

According to the definition of Vorob'ev expectation, the median set of Γ and Π is the 0.5-level set. The mean sets, denoted by $\Gamma_m$ and $\Pi_m$ are defined as:

$$\Gamma_m = \{\xi \in \mathbb{R}^2, 0 \leq p_m \leq 1: \Pr_{\Gamma}(\xi) \geq p_m\}$$

$$\Pi_m = \{\xi \in \mathbb{R}^2, 0 \leq p_m \leq 1: \Pr_{\Pi}(\xi) \geq p_m\}$$

where $p_m$ is determined such that the sets $\Gamma_m$ and $\Pi_m$ have the area EA(Γ) and EA(Π), accordingly. In summary, the Vorob'ev mean of the random sets Γ and Π are estimated by first determining the mean area EA(Γ) and EA(Π), and then finding a p-level set for Γ and Π which having the areas equal to EA(Γ) and EA(Π), accordingly. The p-level is defined for the random set Γ as $\Gamma_p = \{\xi \in \mathbb{R}^2, 0 \leq p \leq 1: \Pr_{\Gamma}(\xi) \geq p\}$. If there is more than one $p_m$ for the random sets than the infimum of all such $p_m$s will be taken.

Set-theoretic variances for the random set Γ and Π are defined as:

$$\Gamma_{var}(\xi) = \sum_{i=1}^{N} (I_{\mathcal{A}_i}(\xi) - \Pr_{\Gamma}(\xi))^2$$

$$\Pi_{var}(\xi) = \sum_{i=1}^{N} (I_{\mathcal{B}_j}(\xi) - \Pr_{\Pi}(\xi))^2.$$

Pixels with variance value equal to 0 are expected in the certain part of an object, whereas high values are expected in the boundary area. The sum of $\Gamma_{var}$, denoted as SD and defined as:

$$SD = pixel\ size * \sum_{\xi \in I} \Gamma_{var}(\xi), \quad \xi \in I \subset \mathbb{R}^2$$

The coefficient of variation (CV) is used as a normalized and dimensionless measure and defined as CV=SD/EA. An extensional uncertainty for GSI and DCA can be identified by:

$$CV = \frac{\sum_{\xi \in I} \Gamma_{var}(\xi)}{\sum_{\xi \in I} \Pr_{\Gamma}(\xi)}$$ - for glacier snow and ice, and

$$CV = \frac{\sum_{\xi \in I} \Pi_{var}(\xi)}{\sum_{\xi \in I} \Pr_{\Pi}(\xi)}$$ - debris-covered area

The CV summarizes the dispersion of the distribution of a random set and allowing us to make comparison with other objects. A high CV indicates a larger proportion of objects with a high $\Gamma_{var}$ or $\Pi_{var}$ and thus points to a large extensional uncertainty.

## 3.7. VALIDATION OF THE RESULTS

To validate the adopted method for uncertainty modelling of a debris-covered glacier reference data are necessary. Due to lack of reference data we will use manually digitized glacier boundary from pan-sharpened Landsat image.

The core set of GSI and DCA will be validated versus the certain area of the glacier by means of confusion matrix (Error of Omission, Producer Accuracy, Error of Commission and User Accuracy). The support and median set cannot be validated by method we were chosen here, as there is no data on fuzziness.

# 4. RESULTS

## 4.1. DEM QUALITY ASSESSMENT

Quality control of DEM is essential for glaciers studies, thus the first step is to assess the quality of SRTM3, interpolated SRTM1 and ASTER GDEM, before they can be applied. Spatial resolution of SRTM3 DEM is 90 m, which obviously is not sufficient for detailed analyses of the terrain. Thus, SRTM3 DEM was re-sampled to SRTM1 DEM with 30 m spatial resolution by cubic convolution method of interpolation.

Quality assessment of SRTM3, SRTM1 and ASTER GDEM against ground control points (GCP) had been performed. The aim is to determine the most suitable DEM to be used in this research for identification of debris-covered areas of the glacier.

By comparing the DEMs with the GCPs it was found that the re-sampled SRTM1 DEM is more accurate than the other two ones. The statistics on quality assessment are given in Table 5 and 6.

Table 5. Statistics on comparison of reference height data with DEMS

| | ASTER GDEM | SRTM3 | SRTM1 |
|---|---|---|---|
| Minimum | -114.35 | -95.35 | -96.35 |
| Maximum | 352.65 | 277.65 | 279.65 |
| Mean | 53.48 | 74.19 | 62.18 |
| Standard Deviation | 84.27 | 79.78 | 76.21 |
| Mean Error | 53.48 | 74.19 | 62.18 |
| **RMSE** | **99.34** | **108.56** | **97.97** |

Table 6. 95% confidence interval for DEMs.

| | ASTER GDEM | SRTM3 | SRTM1 |
|---|---|---|---|
| 95% confidence | 138.61 | 131.23 | 125.35 |

Based on the statistics it is obvious that the re-sampled SRTM1 has a lower RMSE value in comparison with SRTM3 and ASTER GDEM. Also the estimated accuracy of 125.35 meters was found in 95% confidence interval for vertical data, which is better than the two other tested DEMs. Residual distribution of DEMs against heights and slope are given in Figures 13 and 14. The SRTM1 show smaller residuals in comparison with SRTM3 but both DEMs in low altitudes have negative residuals and with increasing of the altitude residuals are also increasing for both DEMs (Figure 16).

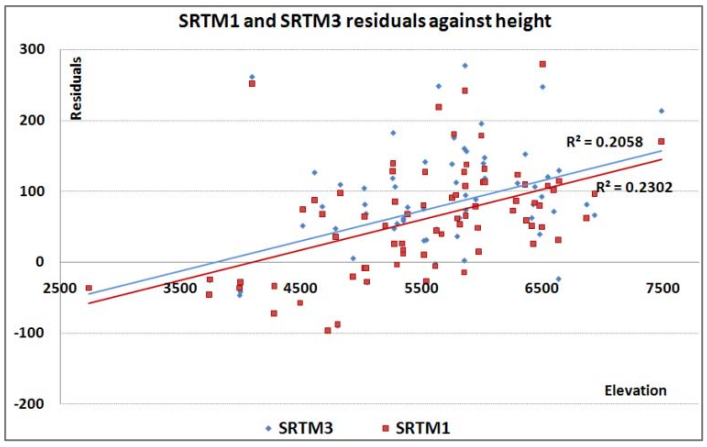


Figure 13. SRTM1 and SRTM3 residuals against height

In steeps slopes the residuals are high and for plain areas the value are negative. Also, the results show that in the less steep areas the residuals are moderate. In this research we are actually interested in the gentle areas (slope: 0° to 24°) and thus the interpolated SRTM1 can be utilized.

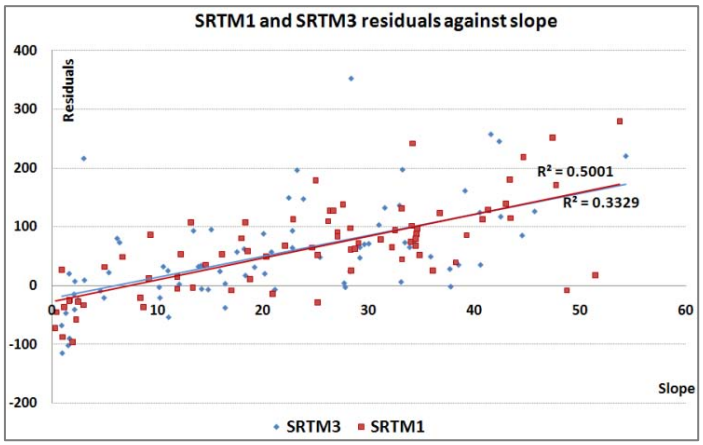


Figure 14. SRTM1 and SRTM3 residuals against slope

ASTER GDEM is not applicable for this research due to the fact that the elevation data are averaged. For the study area all available ASTER stereo scenes were used to produce the data and averaging selected data to create final pixel values. Due to glaciers movement, the glacier surface and especially moraines in the averaged elevation data are not represented correctly – it has very rough surface (Figure 15a, in yellow circle). In comparison with ASTER GDEM the SRTM1 represents the surrounding terrain smoothly and the glacier lateral moraines can be observed (Figure 15b).

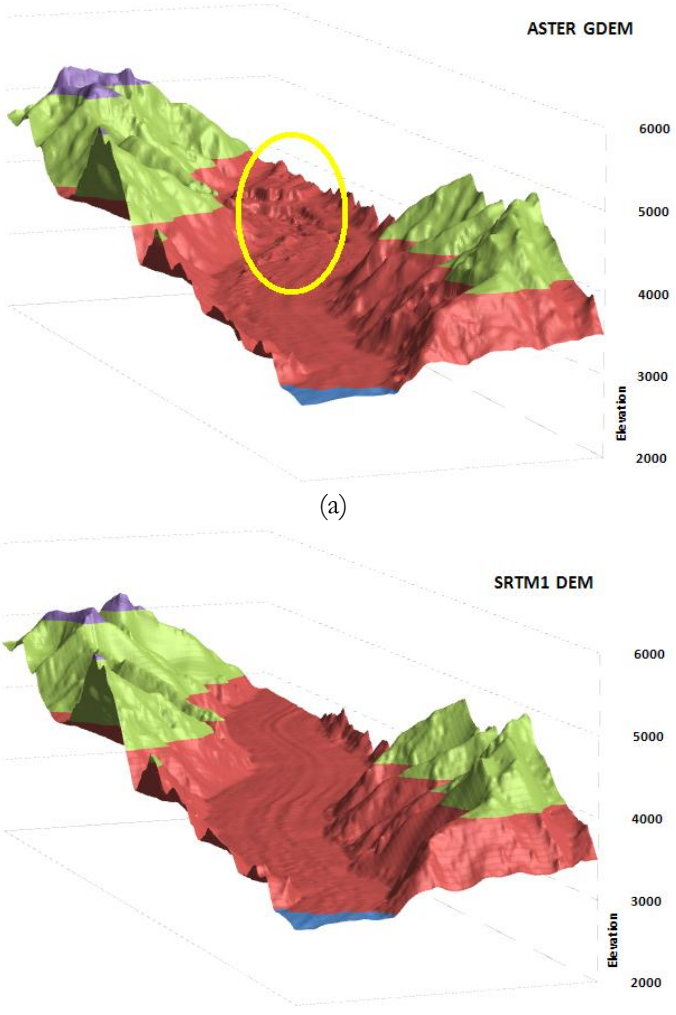


Figure 15. (a) ASTER GDEM and (b) SRTM1 DEM for Fedchenko glacier.

## 4.2. RANDOM SETS GENERATION

**Random set generation for GSI:** The thresholding approach was used to generate GSI random set from an NDSI image. An NDSI image is calculated from Landsat ETM+ imagery acquired on September 1999. We took an NDSI range [0.4, 0.6], step 0.01. The thresholding parameters were selected by detailed inspection of images, as the human eye can estimate the correct values by using textural features and due to the fact that most applied thresholds for NDSI segmentation vary in the range of [0.4, 0.6] (Silverio & Jaquet, 2005),(Racoviteanu, A. E., et al., 2008). This range was divided into 20 equal intervals and 21 thresholds were obtained to slice NDSI images and make samples of binary images (Figure 20). Each sample is realisation of focal elements $\mathcal{A}_i$, $i = \{1,2,..., n\}$, n=21 of GSI.

Samples of binary images extracted from NDSI image by thresholding and their covering function are given below in Figure 19. Each realisation of sample slightly differs from previous or next sample by reason of applying different thresholds. The covering function map (column 2, row 2 in Figure 16) illustrates the probability of pixels being covered by the GSI. A brighter a pixel means there is more probability of a pixel to be GSI. The covering function is calculated by Eq. (1).

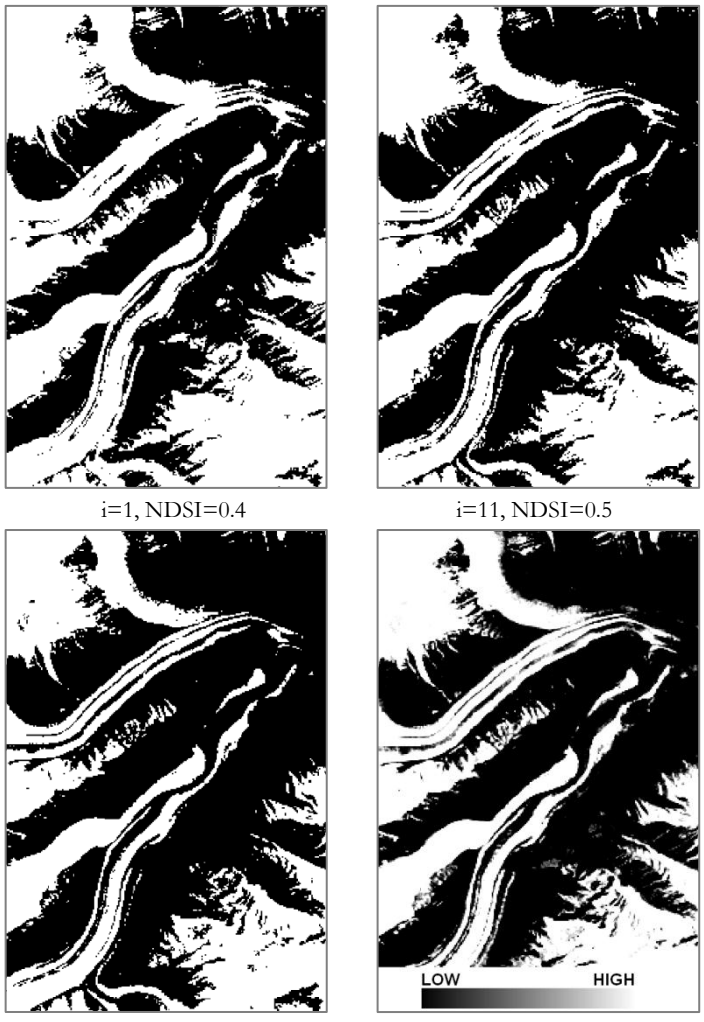


i=1, NDSI=0.4 i=11, NDSI=0.5

i=16, NDSI=0.6 Covering function

Figure 16. Samples of the GSI random set and the covering function.

Binary images: pixels in white indicate glaciated area and pixels in black indicate non-glaciated. Covering function: A brighter a pixel means there is more probability of a pixel to be GSI.

All detached GSI regions with area less than 0.05 km² were eliminated from further set calculation (Figure 17a and 17b, regions within gray circles). By applying a covering function, we generated the random set for GSI: $\Gamma_s = \{\xi \in \mathbb{R}^2 : Pr_\Gamma(\xi) \geq 0\}$.

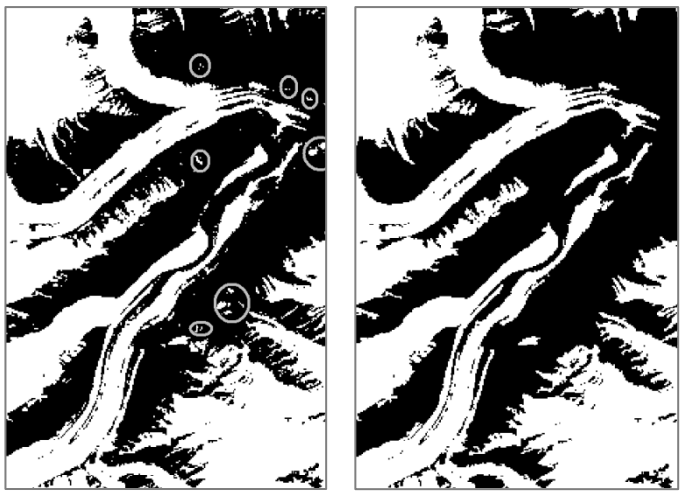

(a) (b)

Figure 17. (a) Support set of GSI, within gray circle regions with area less than 0.05 km2; (b) Processed GSI.

**Random set generation for DCA:** As it was mentioned before, in this research we will use slope information to extract DCA of the glacier. In order to identify the thresholds range and to generate samples of binary images (plane surface – steep surface) the slope information from cross-profiles to the glacier body is utilized (Figure 20). We use two groups of cross-profiles: one from the end part (Figure 18-A1) and another from the middle part (Figure 18-A2) of the glacier.

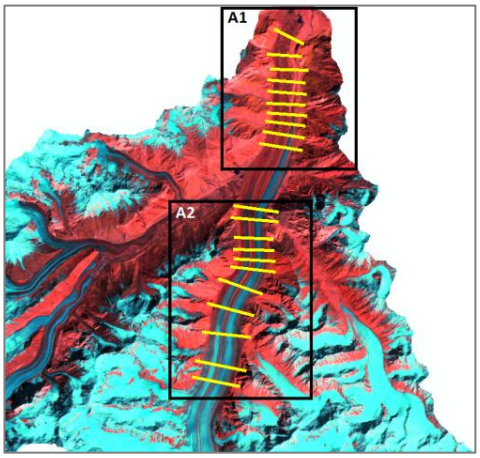


Figure 18. Cross-profiles to the glacier body

The minimum threshold value is taken as the mean slope value from the cross-profile statistic (Table 67 and Figure 19), which is equal to 10.83 (rounded to 11). Thereby, a plain area under 11° in the study area is considered to be DCA with no uncertainty. The maximum threshold value is chosen as 24 to cover steeper areas where DCA of the glacier might occur (Paul, F., et al., 2004). The identified range of threshold values [11, 24] will be divided into 28 equal intervals and 29 thresholds obtained to slice the slope images and make samples of binary images. Each sample will be realisation of a focal elements $\mathcal{B}_j$, $j = \{1, 2, ..., m\}$, of the DCA random region.

Table 7. Cross-profiles statistics.

| MIN | MAX | MEAN | SD |
|---|---|---|---|
| 0 | 62.09 | 10.83 | 12.84 |

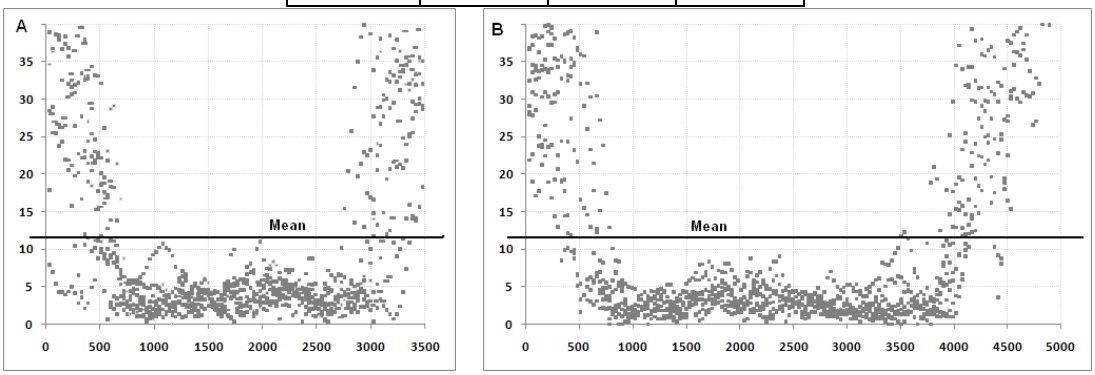


Figure 19. Scatter plot of all slope profiles from two groups of cross-profiles taken perpendicular to the flow direction (x axis – cross-profiles sample distance in meters, y – slope).

The extracted binary images from slope image by thresholding and their covering function are given below in Figure 20. The covering function map (column 2, row 2 on Figure 22) illustrates the probability of pixels being covered by DCA.

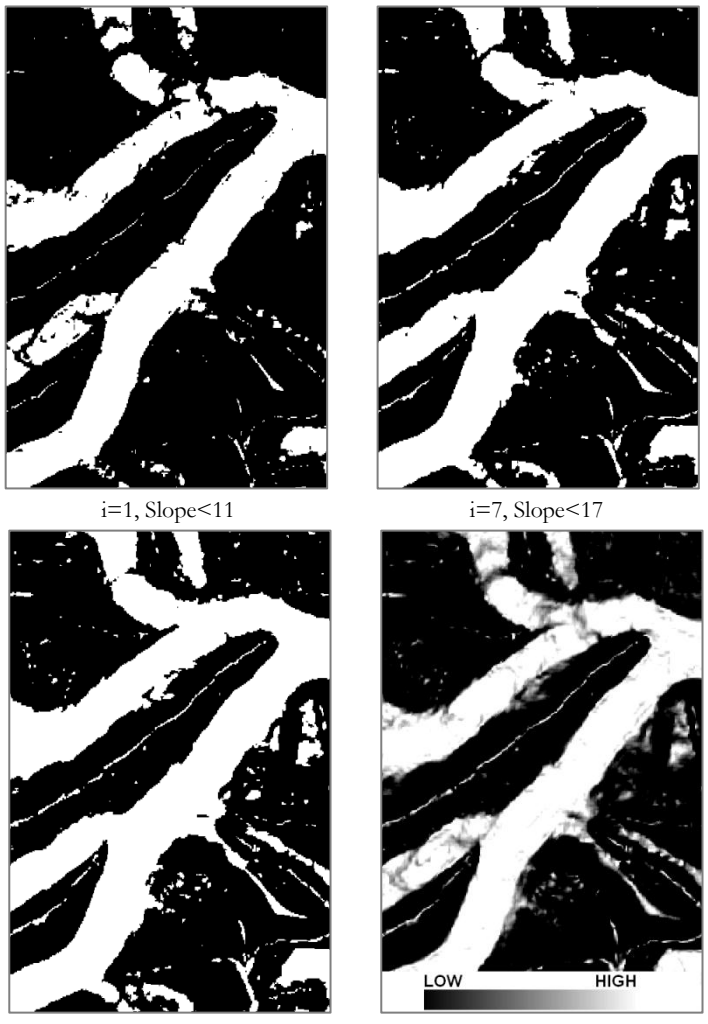


i=1, Slope<11 i=7, Slope<17

i=14, Slope<20 Covering function

Figure 20. Samples of the DCA random set and the covering function.

Binary images: pixels in white indicate DCA and pixels in black indicate non-DCA. Covering function: A brighter a pixel means there is more probability of a pixel to be DCA.

Based on the methodology described in chapter 3, before to generate a random set for DCA, all detached DCA regions which did not overlap with GSI regions were eliminated (Figure 21). Thereafter, by applying a covering function, we generated the random set for DCA: $\Pi_s=\{\xi \in \mathbb{R}^2: Pr_{\Gamma}(\xi)\geq 0\}$.

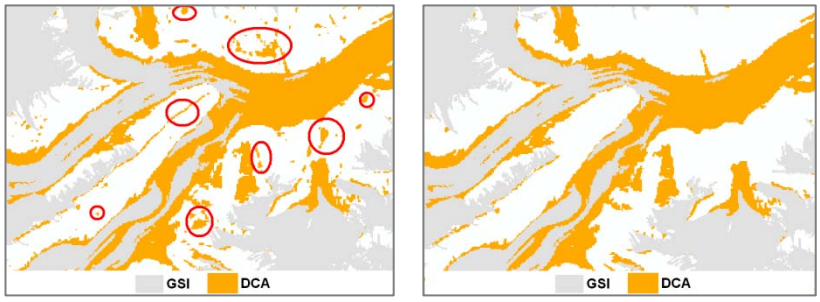


(a) (b)

Figure 21. (a) Detached areas are in red circle. (b) Eliminated detached areas .

The median set of Π was used to recalculate a probability value for DCA regions which did not overlap with GSI and had a high probability (more than 0.5) of being a part of DCA. The idea was to downgrade the probability for such kind of regions. In Figure 23-b within red circles the DCA regions are indicated which probabilities were recalculated.

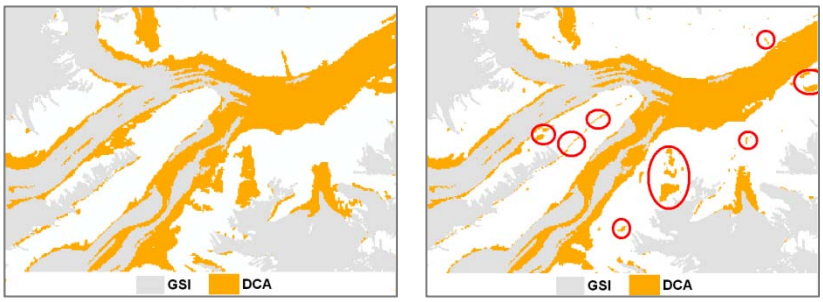


(a) (b)

Figure 22. (a) Support set of Π (DCA). (b) Detached DCA area of median set of Π (in red circle).

Last step was a recalculation of elements probability for the random set Π which were covered by GSI. We used the below condition to recalculate a probability for elements of Π:

IF $Pr_{\Gamma}(\xi)>0$ (Figure 23-a, coloured areas) AND $Pr_{\Pi}(\xi)>0$ (Figure 23-b, gray areas)

THAN $Pr_{\Pi}(\xi)=1 - Pr_{\Gamma}(\xi)$ (Figure 23-c, coloured areas).


(a) (b) (c)

Figure 23. (a) Support set of Π (DCA), (b) Support set of Γ (GSI), (c) Recalculated support set of Π (DCA).

The resulting random set Π for DCA is mapped in Figure 24-c and included those areas (1) which are connected to GSI regions and (2) which elements were recalculated.

## 4.3. UNCERTAINTY QUANTIFICATION

The results of a random set application for uncertainty quantification of a debris-covered glacier are discussed in this section. The random sets Γ and Π were generated to calculate the area covered by GSI and DCA and to estimate the main characteristics of the random sets Γ and Π, including the covering function, the support, median and core sets and the variance.

The area of mean, median and core sets of Γ and Π are given in Table 8.

Table 8. Mean, median and core seta area for GSI and DCA.

| Area ($km^2$) | GSI | DCA | Total |
|---|---|---|---|
| Mean set (p=0) | 841.87 | 94.39 | **936.26** |
| Median set (p=0.5) | 834.90 | 84.71 | **919.61** |
| Core set(p=1) | 791.09 | 61.36 | **852.44** |

The p-level sets area dynamic change is shown in Figure 24 and 25. It is a function of p-level set ($0 \leq p \leq 1$) and its area. The p-level sets area decreases, when $p \rightarrow 1$.

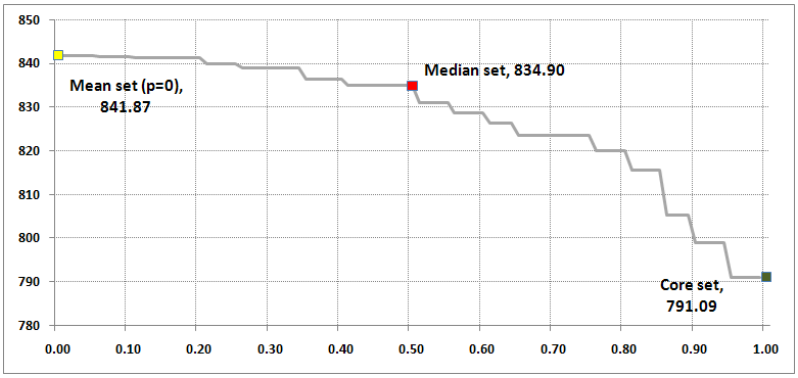


Figure 25. p-level set area dynamic change for GSI: x – p-level, y – area in km².

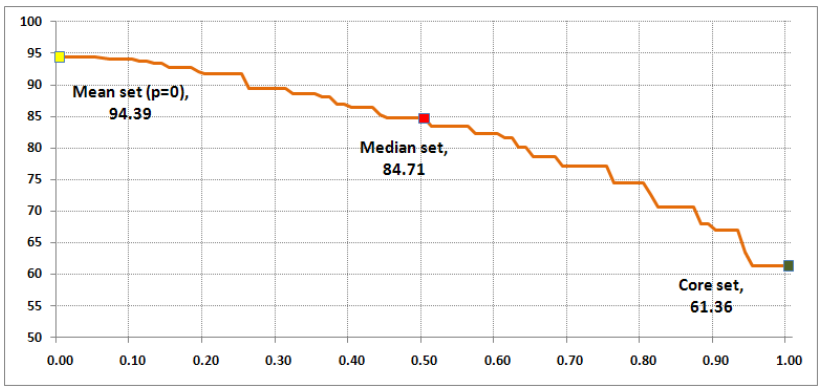


Figure 26. p-level set area dynamic change for DCA: x – p-level, y – area in km².

Table 9 shows that the area of p-level set ($0.5 \leq p < 1$) is quite larger in comparison with p-level set area defined as ($0 < p < 0.5$). It is an indication of the fact that more uncertain area of GIS and DCA are within the median-level set. It is obvious that 86.27% of extensional uncertainties of GSI and 70.69% of DCA are within 0.5-level set (Table 9). The rest of uncertain area of GSI (13.73) and DCA (29.31) are within p-level set ($0 < p < 0.5$).

Table 9. The uncertain area sets area changes.

| p-level set | GSI | | DCA | |
|---|---|---|---|---|
| | $km^2$ | % | $km^2$ | % |
| Core to Median (0.5≤p<1) | 43.81 | 86.27 | 23.35 | 70.69 |
| Median to Support (0<p<0.5) | 6.97 | 13.73 | 9.68 | 29.31 |
| **Total** | **50.78** | **100.00** | **33.03** | **100.00** |

To estimate the extensional uncertainty we used the sum of set-theoretical variance (SD) and the coefficient of variation (CV) indicators, allowing us to summarize the dispersion of a random set and to make comparisons with other objects. The differences between the spatial extension of support set and core set indicate the extensional uncertainty. The higher uncertainty corresponds to a higher variance of the random set Γ and Π in Figure 26. We found that CV is 0.021 for GSI and for DCA: CV=0.2.

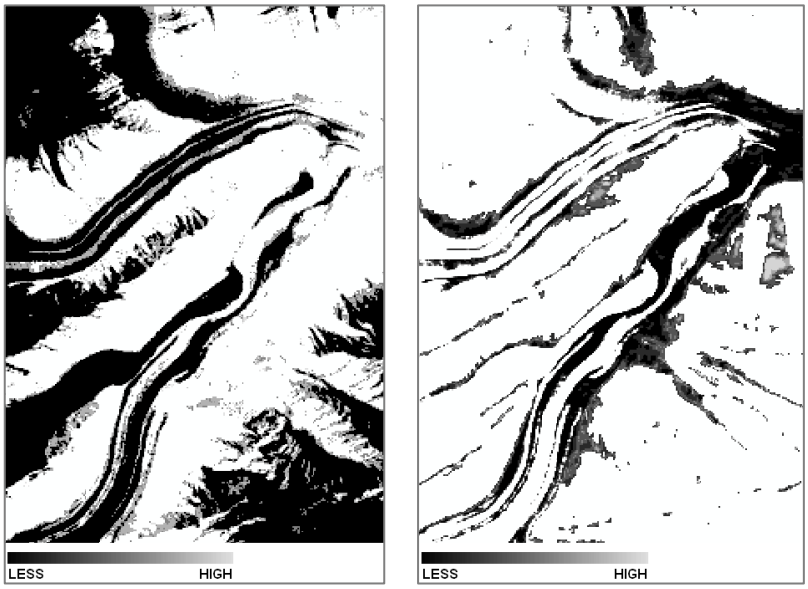


(a) (b)

Figure 27. Extensional uncertainty described by concepts of set-theoretical variance: (a) GSI, (b) DCA

Due to the rough mountainous terrain of debris-covered glaciers, each of a terrain aspect has specific properties, for example there is more snow accumulation in north aspect of a terrain due to less solar illumination in comparison with the south aspect. Thus we used the aspect information derived from SRTM1 DEM to quantify the uncertainty of GSI and DCA. The results are given below Table 10.

Table 10. Variation of GSI and DAC versus aspect

| Aspect | Study area ($km^2$) | GSI | | | DCA | | |
|---|---|---|---|---|---|---|---|
| | | Mean area ($km^2$) | SD | CV | Mean area ($km^2$) | SD | CV |
| Flat | 1.92 | 2.09 | 0.017 | 0.008 | 0.32 | 0.021 | 0.067 |
| N | 273.75 | 184.95 | 1.861 | 0.010 | 17.63 | 2.696 | 0.153 |
| NE | 215.86 | 140.22 | 1.752 | 0.012 | 15.13 | 2.307 | 0.152 |
| E | 153.87 | 90.94 | 1.702 | 0.019 | 12.97 | 2.374 | 0.183 |
| SE | 176.83 | 88.46 | 2.531 | 0.029 | 10.59 | 2.552 | 0.241 |
| S | 196.51 | 94.52 | 3.620 | 0.038 | 7.65 | 2.107 | 0.275 |
| SW | 150.15 | 62.78 | 2.390 | 0.038 | 6.47 | 1.990 | 0.308 |
| W | 126.69 | 63.70 | 1.786 | 0.028 | 8.52 | 2.111 | 0.248 |
| NW | 196.87 | 115.32 | 2.083 | 0.018 | 15.07 | 2.499 | 0.166 |
| **TOTAL** | **1492.45** | **841.87** | **17.780** | **0.021** | **94.39** | **18.71** | **0.20** |

Allocation of GSI and DCA of the glacier versus aspects is proportionally to the total area of terrain aspects (Figure 27-a). More GSI areas were detected on the north aspect due to the meridian allocation of the Fedchenko glacier and partly because of less solar illumination reaching the glacier surface. One of the biggest tributary of the Fedchenko glacier flows to the NE direction and a large portion of its covered by debris, thus DCAs were mostly detected in NE and N aspect of the terrain (Figure 27-b).

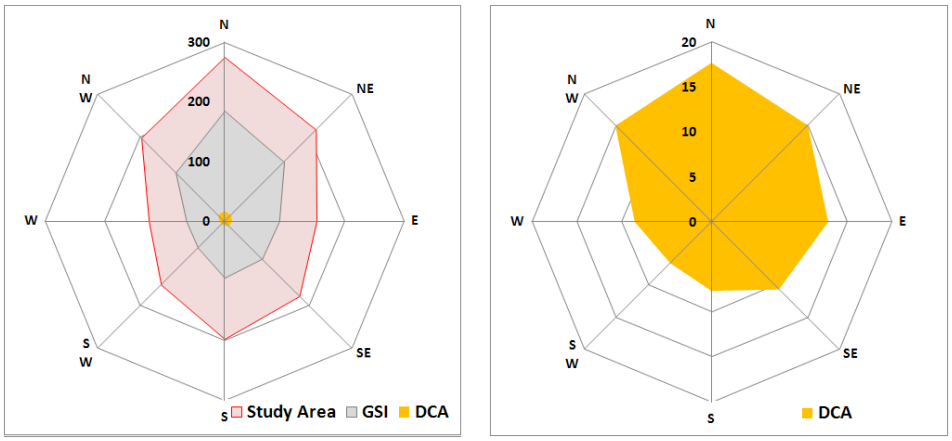


(a) (b)

Figure 28. (a) Diagrams showing allocation of GSI and DCA versus aspect for the whole study area (b) DCA allocation versus aspect

A large extensional uncertainty of GSI were detected on the south-western and south aspects of the terrain (CV=0.038) and less on the north aspect (CV=0.01). Whereas the sun azimuth (143.55) and sun elevation (51.93) of ETM+ image used in this research, the reason of comparative large extensional uncertainty might be saturated pixels on southward aspects (Figure 28). The total CV for GSI is 0.021 which is an indicator of a less extensional uncertainty. For DCA a quite large extensional uncertainty was detected (CV=0.2), and most of DCAs occur on SW and South aspects. The reason of such a large uncertainty is in a rough mountainous terrain.

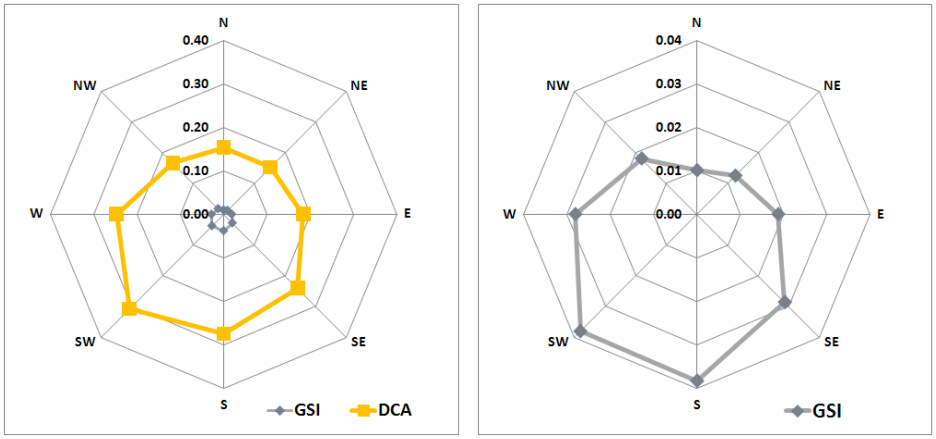


Figure 29. CV of GSI and DCA areas versus aspect.

## 4.4. TEMPORAL CHANGES

For temporal analysis we used three images (date of acquisition: 1992, 1999, 2009) from Landsat TM and ETM+ sensors. The temporal DEM for the study area was only available from February 2000. Thus, to perform temporal analysis we made an assumption that DCA of the glacier is not changed from 1992 to 2009.

The idea is to show the change in a debris-covered glacier extent and to quantify the uncertainties. The support set, the mean and the core set areas of GSI and DCA and CV were estimated. The results are given below in Table 11.

Table 11. The mean, median and core set areas of GSI and DCA per years.

| Year | GCI area ($km^2$) | | | DCA area ($km^2$) | | | Total area ($km^2$) | | |
|---|---|---|---|---|---|---|---|---|---|
| | Mean | Median | Core | Mean | Median | Core | Mean | Median | Core |
| 1992 | 742.78 | 738.39 | 708.26 | 121.89 | 110.83 | 85.73 | 864.67 | 849.22 | 793.99 |
| 1999 | 841.87 | 834.90 | 791.09 | 94.39 | 84.71 | 61.36 | 936.26 | 919.61 | 852.44 |
| 2009 | 800.89 | 794.77 | 750.66 | 108.87 | 98.87 | 75.80 | 909.75 | 893.64 | 826.46 |

The core set area is the certain area of the glacier (GCI and DCA). The total uncertain area of median and mean set in percentage is given in Table 12. There is more uncertainty in DCA in comparison with GSI or more variation between core set and mean set of Γ and Π. The maximum uncertain area (difference between the support set and mean set) for GSI was found for 2009 and it makes up 6.27% from the total area (Table 12).

Table 12. Percentage of uncertainly areas for GSI and DCA.

| Year | GCI uncertain area (%) | | | DCA uncertain area (%) | | | Total uncertain area (%) | | |
|---|---|---|---|---|---|---|---|---|---|
| | Mean | Median | Core | Mean | Median | Core | Mean | Median | Core |
| 1992 | 4.65 | 4.08 | 0.00 | 29.67 | 22.65 | 0.00 | 8.17 | 6.50 | 0.00 |
| 1999 | 6.03 | 5.25 | 0.00 | 34.99 | 27.56 | 0.00 | 8.95 | 7.30 | 0.00 |
| 2009 | 6.27 | 5.55 | 0.00 | 30.37 | 23.33 | 0.00 | 9.16 | 7.52 | 0.00 |

The area of GSI increased in size from 1992 to 1999 and is decreasing since 1999 which graphically is shown in Figure 29.

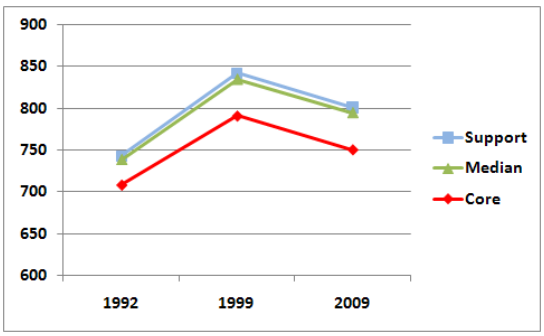


Figure 30. Mean, median and support areas for GSI.

The DCA of the glacier decreased from 1992 to 1999 and is decreasing since 1999 (Figure 30). That is because of snow and ice melting or accumulation process occurring on glaciers surface. If GSI melts it leaves the buried debris of glacier bared. But the uncertain area in DCA in comparison with GSI is quite large. Maximum uncertainty in DCA area was detected in 1999, which makes up 34.99% from the total DCA area (Table 12).

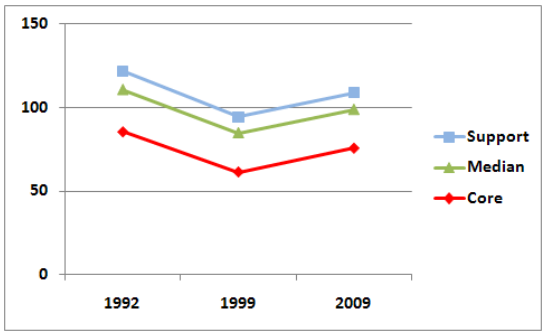


Figure 31. Mean, median and support areas for DCA.

The variation of uncertainty in term of CV for GSI and DCA is given in Table 13 and plotted in Figure 30.

Table 13. The variation of uncertainty of temporal data

| Year | GCI | | | DCA | | | Total glacier area ($km^2$) |
|---|---|---|---|---|---|---|---|
| | Mean area ($km^2$) | SD | CV | Mean area ($km^2$) | SD | CV | |
| 1992 | 742.78 | 32.727 | 0.044 | 121.89 | 18.001 | 0.148 | 864.67 |
| 1999 | 841.87 | 17.780 | 0.021 | 94.39 | 18.706 | 0.198 | 936.26 |
| 2009 | 800.89 | 17.535 | 0.022 | 108.87 | 18.316 | 0.168 | 909.75 |

The results show that the uncertainty in GSI extent is much less in comparison with DCA. As we used slope information for DCA identification and a mountainous terrain of the glacier is quite rough, it affects the quality of DCA classification, thus there is more extensional uncertainty in DCA.

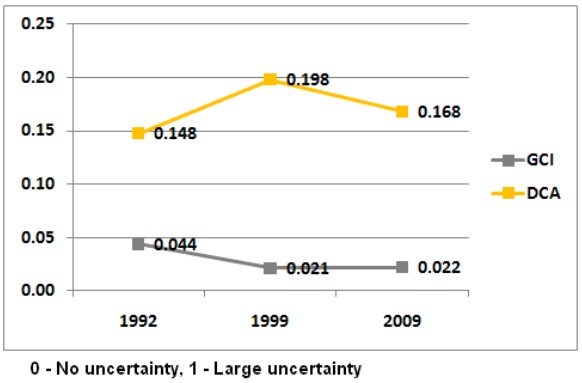


Figure 32. Coefficient of variance (CV) for GSI and DCA.

The glacier area change from 1992 to 2009 and uncertainty quantification in term of CV versus aspect are given in Figure 31 and 32. It was observed that when the GSI area of glacier decreases the DCA increases (Figure 31-a and 31-b), that is because of snow and ice melting process which causes striping of debris.

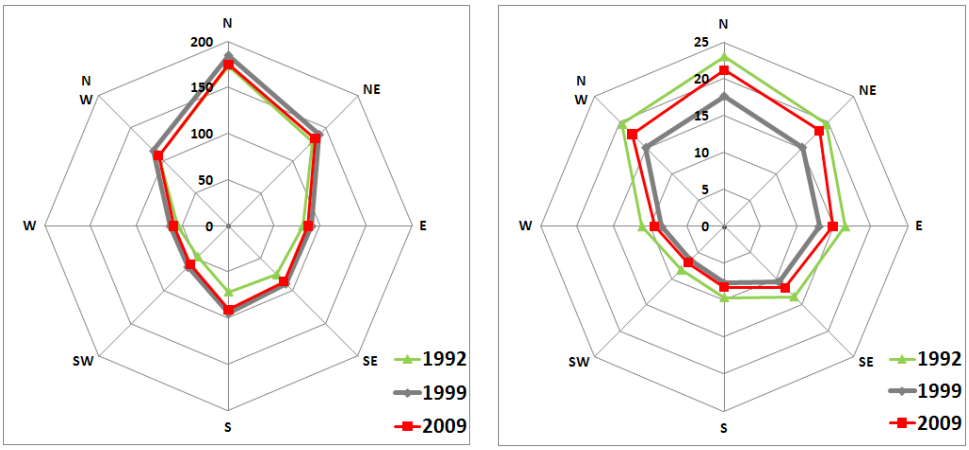


(a) (b)

Figure 33. Fedchenko area change from 1992 to 2009: (a) GSI, (b) DCA

Temporal analysis performed in this research show that an uncertainty variation in DCA depends on uncertainty in GSI, as melting or accumulation of snow and ice affects a glacier area covered by debris. In 1992, there was less extensional uncertainty in GSI but more extensional uncertainty in DCA (Figure 32-a and 32-b).


(a) (b)

Figure 34. Temporal analysis: CV of (a) GSI and (b) DCA areas versus aspect.

## 4.5. VALIDATION

To validate the method proposed in this research we used the digitized boundaries of the glacier as a reference data. As the study area covers a wide glaciated area we used two different areas for validation. We tried to test the method for different areas in order to take into consideration the terrain location variation and roughness. Here we validate the core set of debris-covered areas only, as there is no field data for support and median set. The digitized boundaries are considered to be a core set of debris-covered area of the glacier.

The areas for validation are marked as A in B in Figure 33.

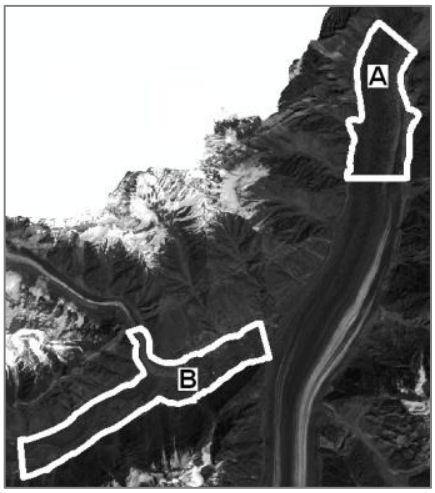


Figure 35. Validation areas

The area A is located in end part of the glacier and its surface is moderately plain. But for the area B the situation is inversed.

The results of validation are given below for two area (A) and (B).

| A | Reference Data | | Total | Error of Commission (%) | User Accuracy (%) |
|---|---|---|---|---|---|
| | DCA | misc. | | | |
| DCA | 7528 | 0 | 7528 | 0 | 100 |
| misc. | 1068 | 0 | 1068 | 0 | 100 |
| **Total** | **8596** | **0** | **8596** | | |
| Error of Omission (%) | 12.42 | 0 | 87.58% | | |
| Producer Accuracy (%) | 87.58 | 0 | | | |

| B | Reference Data | | Total | Error of Commission (%) | User Accuracy (%) |
|---|---|---|---|---|---|
| | DCA | misc. | | | |
| DCA | 8156 | 0 | 8156 | 0 | 100 |
| misc. | 2873 | 0 | 2873 | 0 | 100 |
| **Total** | **11029** | **0** | **11029** | | |
| Error of Omission (%) | 26.05 | 0 | 73.95% | | |
| Producer Accuracy (%) | 73.95 | 0 | | | |

Overall accuracy for area (A) is 87.58% for the core set of the DCA. For area (B) the accuracy is 73.5% due to the terrain roughness.

# 5. DISCUSSION

A debris-covered glacier as a spatial object with inherent uncertainty practically cannot be extracted effectively from satellite images by means of crisp-based classification, as these methods ignore uncertain areas or transition zones. Fuzzy classification method allows to model uncertainties of spatial objects by mean of membership functions, but due to the fact that the assignment of the membership function is subjective in nature, a major obstacle of fuzzy set approach is determination of the membership function (Robinson, 2003). In this research, therefore, we proposed a spatial data model based on random set theory for uncertainty modelling of debris-covered glaciers. The applicability of the method is discussed in detail in this chapter.

We applied a random set model for uncertainty modelling of a debris-covered glacier. The uncertainties were modelled for glacier snow and ice and for debris-covered areas of a glacier separately. This partitioning allowed us to quantify the uncertainty for both constitute part of a glacier. This is very important as in some cases glacier areas covered by debris constitute a large part of glacier surface and theirs ignoring will lead to the misclassification. For example in this research we found that about 10% of Fedchenko glacier is covered by debris.

By using the statistical parameters of random sets (support, mean, median, variance) we demonstrated the randomness of segmentation thresholding parameters has different effects on extracted snow and ice and debris-covered areas. Random sets were generated based on range of thresholding parameters, thus the selection of thresholds must be performed carefully. Uncertainties modelling for glacier snow and ice require less processing steps (chapter 3.5.2) as we used an NDSI image for generation of focal elements for a random set. Debris-covered areas were identified based on slope information. Due to a rough mountainous terrain of a glacier, we made some pre-processing steps to generate a random set for debris-covered area prior to perform statistical analysis (chapter 3.5.2).

The mean, median and core sets area were calculated for glacier snow and ice, and debris-covered area and it was found that the significant uncertain area is located within 0.5-level set for both of GSI and DCA. For estimation of extensional uncertainty we used coefficient of variation (CV) indicator. It was found that there is less extensional uncertainty (CV=0.02) for snow and ice areas in comparison to debris-covered areas (CV=0.2). Such a big uncertainty for debris-covered areas can be explained by terrain heterogeneity of the study area and the presence of plain areas closely located to the glacier body and which is identified as a part of it (chapter 3.5.2).

Taking the rough mountainous terrain of the glacier into account we quantified the uncertainty versus aspects and found that in southward direction of the terrain, the extensional uncertainty is twice larger in comparison to northward direction, for both component of the glacier (chapter 4.3). The largest CV for snow and ice were detected in the south and southwest aspects, despite the fact that there are fewer amounts of accumulated snow and ice. The reason of such variation is the presence of saturated pixels on the terrain aspects exposed to sunlight.

Temporal analysis of the glacier by uncertainty modelling shown that the mean area of snow and ice increased from 1992 to 1999 and it is decreasing since 1999 in opposite to the debris-covered area. The correlation between ice and snow and debris-covered glacier area can be interpreted by the fact that when

the ice or snow melts it lives buried debris bared. The end part of a glacier or glacier terminus was digitized manually, as it was not impossible to detect the terminus by slope data (low spatial resolution) we used in this research. Temporal analysis performed in this research was shown that an uncertainty variation in debris-covered area depends on uncertainty in glacier snow and ice areas, as melting or accumulation of snow and ice affect glacier areas which are covered by debris (chapter 4.4).

The results of validation revealed that the proposed method is relatively accurate. Due to lack of validation data for uncertain area (support set, median and mean set) we validated only core set of debris-covered areas. Overall accuracy is 87.58% and 73.5% for two tested areas (chapter 4.5).

In this research due to unavailability of temporal DEM, we made an assumption that debris-covered areas of the glacier were not changed from 1992 to 2009 in order to perform time-series analysis. But in fact, this happens very rarely, and a glacier moves in the downward direction. Thus, ideally for time-series analysis of debris-covered glacier the availability of temporal DEM is necessary. The biggest challenge for the research method was the lack of field-data for validation. Due to remoteness of most mountainous glaciers, including the research study case, the collecting of field data in short time is not realistic. For validation of uncertainty modelling method we need data describing uncertainties of spatial objects in term of belonging to the certain objects from the field. But for temporal modelling of uncertainties such data might not be available. Ideally, time-series satellite images, DEM and field data are necessary to run the research model.

The method proposed in this research is mainly addressed for uncertainty modelling of debris-covered glaciers. But the method can be applied for uncertainty modelling of glaciers which do not have debris-covered areas. In this case the section 3.5.3 of the methodology has to be skipped. Generally, the proposed method is one way of application of a random set method for uncertainty modelling of spatial objects. (Zhao, et al., 2010) applied the method for uncertainty modelling of vegetation patches by thresholding of NDVI image. Other possible application is using band ratio techniques for identification of glacier snow and ice, for example Landsat TM2/TM5 or TM4/TM5. In general image classification techniques based on thresholding or segmentation methods can be used for spatial objects uncertainty modelling.

# 6. CONCLUSION AND RECOMMENDATION

The main objective of this study was to develop a method for uncertainty modelling of debris-covered glaciers by means of a random set model.

The results of the uncertainty modelling for debris-covered glaciers proved that a random set is an effective tool for modelling and quantification of uncertainties not only for debris-covered areas of glaciers but also for snow and ice. The advantage of the method is in assessing and quantification of the uncertainties inherent to debris-covered glaciers. Thus, the proposed method can be used for accurate assessment of debris-covered glaciers and theirs changes in time which is of vital importance for the planning and management of water resources.

The proposed method is the first attempt to measure and quantify the uncertainties of debris-covered glacier and it needs to be improved further. Especially, there are imperfections in uncertainty modelling of a debris part of a glacier due to the presence of rough glacier surface. Glacier lateral and terminus moraines can be used for improving of detection of debris-covered areas and theirs uncertainly modelling, if they can be observed on DEM.

The limitations of the research method are the following: (1) a rough mountainous terrain disturbs the uncertainty measurement for debris-covered areas of a glacier; (2) the terminus part of a glacier cannot be identified due to absence of steep slope; (3) a presence of flats area wrongly classified as a debris-covered area of a glacier.

In order to address the limitations following is recommended. The fine-resolution DEM is needed for extraction of detailed slope and curvature images and for identification of glacier moraines, which can be used for detection of terminus part of a glacier and elimination of misclassified debris-covered areas.

# LIST OF REFERENCES


Aizen, V. B., & Mayewski, P. A. (2009). *Stable-isotope and trace element time series from Fedchenko glacier (Pamirs) snow/firn cores* (Vol. 55). Cambridge, ROYAUME-UNI: International Glaciological Society.

Albert, T. H. (2002). Evaluation of Remote Sensing Techniques for Ice-Area Classification Applied to the Tropical Quelccaya Ice Cap, Peru. *Polar Geography, 26*(3), 210 - 226.

Andreassen, L. M., Paul, F., & Hausberg, J. E. (2008). Landsat-derived glacier inventory for Jotunheimen, Norway, and deduced glacier changes since the 1930s. *The Cryosphere, 2*, 131 - 145.

Bayr, K. J., Hallb, D. K., & Kovalickc, W. M. (1994). Observations on glaciers in the eastern Austrian Alps using satellite data *International Journal of Remote Sensing, 15*(9), 1733 - 1742

Bennett, M. R., & Glasser, N. F. (1996). *Glacial geology: ice sheets and landforms*: Wiley.

Bishop, M., Bonk, R., Kamp, U., & Shroder, J. (2001). Terrain analysis and data modelling for alpine glacier mapping. *Polar Geography, 25*, 182-201.

Bolch, T. (2007). Climate change and glacier retreat in northern Tien Shan (Kazakhstan/Kyrgyzstan) using remote sensing data. [doi: DOI: 10.1016/j.gloplacha.2006.07.009]. *Global and Planetary Change, 56*(1-2), 1-12.

Bolch, T., & Buchroithner, M. (2007). An Automated Method to Delineate the Ice Extension of the Debris-Covered Glaciers at Mt. Everest Based on ASTER Imagery. [Article]. *Grazer Schriften der Geographie und Raumforschung, 43*, 71-78.

Bolch, T., Buchroithner, M., Pieczonka, T., & Kunert, A. (2008). Planimetric and volumetric glacier changes in the Khumbu Himal, Nepal, since 1962 using Corona, Landsat TM and ASTER data. [Article]. *Journal of Glaciology, 54*(187), 592-600.

Bolch, T., & Kamp, U. (2006). Glacier Mapping in High Mountains Using DEMs, Landsat and ASTER Data. *Grazer Schriften der Geographie und Raumforschung, 41*, 37-48.

Dilo, A., De By, R. A., & Stein, A. (2007). A system of types and operators for handling vague spatial objects. *International Journal of Geographical Information Science, 21*(4), 397-426.

Dozier, J. (1989). Spectral Signature of Alpine Snow Cover from the Landsat Thematic Mapper *Remore Sensing of Environment, 28*, 9 - 22.

Gao, J., & Liu, Y. (2001). Applications of remote sensing, GIS and GPS in glaciology: a review. *Progress in Physical Geography, 25*(4), 520-540.

Haeberli, W., & Epifani, F. (1986). Mapping the distribution of buried ice. *Allllals of Glaciology, 8* 78 - 81.

Haeberli, W., Frauenfelder, R., Hoelzle, M., & Maisch, M. (1999). On rates and acceleration trends of global glacier mass changes. *Geografiska Annaler Series a-Physical Geography, 81A*(4), 585-591.

Hall, D. K., Riggs, A., & Salomonson, V. (1995). Development of methods for mapping global snow cover using moderate resolution imaging spectroradiometer data. *Remote Sensing of Environment, 54*(2), 127-140.

Hall, D. K., Williams, R. S. J., & Bayr, K. J. (1992). Glacier recession in Iceland and Austria. *EOS, Transactions of the American Geophysical Union 73*.

Hendriks, J. P. M., & Pellikka, P. (2007). Semi-automatic glacier delineation from Landsat imagery over Hintereisferner in the Austrian Alps. *Zeitschrift fürgletscherkunde und glazialgeologie, 41*.

Iwata, S. (2009). Mapping Features of Fedchenko Glacier, the Pamirs, Central Asia from Space. *Geographical Studies, 84*, 33 - 43.

Kääb, A. (2005). Combination of SRTM3 and repeat ASTER data for deriving alpine glacier flow velocities in the Bhutan Himalaya. [doi: DOI: 10.1016/j.rse.2004.11.003]. *Remote Sensing of Environment, 94*(4), 463-474.

Kääb, A., Paul, F., Maisch, M., Hoelzle, M., & Haeberli, W. (2002). The new remote-sensing-derived Swiss glacier inventory: II. First results. In J. G. Winther & R. Solberg (Eds.), *Annals of Glaciology, Vol 34, 2002* (Vol. 34, pp. 362-366). Cambridge: Int Glaciological Soc.

Kargel, J. S., Abrams, M. J., Bishop, M. P., Bush, A., Hamilton, G., Jiskoot, H., Kääb, A., Kieffer, H. H., Lee, E. M., Paul, F., Rau, F., Raup, B., Shroder, J. F., Soltesz, D., Stainforth, D., Stearns, L., & Wessels, R. (2005). Multispectral imaging contributions to global land ice measurements from space. *Remote Sensing of Environment, 99*(1-2), 187-219.

Keeratikasikorn, C., & Trisirisatayawong, I. (2008). Reconstruction of 30m DEM from 90m SRTM DEM with bicubic polynomial interpolation method. *The International Archives of the Photogrammetry, Remote Sensing and Spatial Information Sciences, 37*, 791 - 794.

Keshri, A. K., Shukla, A., & Gupta, R. P. (2009). ASTER ratio indices for supraglacial terrain mapping. *International Journal of Remote Sensing, 30*(2), 519 - 524.

Kotlakov, V. M., Osipova, G. B., & Tsvetkov, D. G. (2008). Monitoring surging glaciers of the Pamirs, central Asia, from space. *Annals of Glaciology, 48*, 125 - 134.

Lougeay, R. (1974). Detection of buried glacial and ground ice with thermal infrared remote sensing. *Advanced concepts and techniques in the study of snow and ice resources*, 487 - 494.

Lucieer, A., & Stein, A. (2002). Existential uncertainty of spatial objects segmented from satellite sensor imagery. *Geoscience and Remote Sensing, 40*(11), 2518-2521.

Mahler, R. (2007). *Statistical multisource-multitarget information fusion*. Norwood, MA, USA: Artech House, Inc.

Masek, J. (2010). Lansat 7: Science Data Users Handbook. Retrieved December, 21, 2010, from http://landsathandbook.gsfc.nasa.gov/handbook/handbook_toc.html

Negi, H. S., V., K. A., & Semwal, B. S. (2009). Estimation of snow cover distribution in Beas basin, Indian Himalaya using satellite data and ground measurements. *Earth Syst. Sci., 118*, 525–538.

Paul, F., & Andreassen, L. M. (2009). A new glacier inventory for the Svartisen region, Norway, from Landsat ETM+ data: challenges and change assessment. *Journal of Glaciology, 55*(192), 607 - 618.

Paul, F., Huggel, C., & Kaab, A. (2004). Combining satellite multispectral image data and a digital elevation model for mapping debris-covered glaciers. *Remote Sensing of Environment, 89*(4), 510-518.

Paul, F., Huggel, C., & Kääb, A. (2002). Comparison of TM-derived glacier areas with high resolution data sets.

Paul, F., Kääb, A., Maisch, M., Kellenberger, T., & Haeberli, W. (2002). The new remote-sensing-derived swiss glacier inventory: I. Methods. *Annals of Glaciology, 34*, 355-361.

Paul, P. (2000). Evaluation of different methods for glacier mapping using Landsat TM. Dresden.

Rabus, B., Eineder, M., Roth, A., & Bamler, R. (2003). The shuttle radar topography mission—a new class of digital elevation models acquired by spaceborne radar. *ISPRS Journal of Photogrammetry & Remote Sensing, 57*, 241 - 262.

Racoviteanu, A. E., Arnaud, Y., Williams, M. W., & Ordonez, J. (2008). Decadal changes in glacier parameters in the Cordillera Blanca, Peru, derived from remote sensing. *Journal of Glaciology, 54*, 499-510.

Racoviteanu, A. E., Manley, W. F., Arnaud, Y., & Williams, M. W. (2007). Evaluating digital elevation models for glaciologic applications: An example from Nevado Coropuna, Peruvian Andes. *Global and Planetary Change, 59*(1-4), 110-125.

Racoviteanu, A. E., Paul, F., Raup, B., Khalsa, S. J., & Armstrong, R. (2009). Challenges and recommendations in mapping of glacier parameters from space: results of the 2008 Global Land Ice Measurements from Space (GLIMS) workshop, Boulder, Colorado, USA. *Annals of Glaciology, 50*(53), 53 - 69.

Racoviteanu, A. E., Williams, M. W., & Barry, R. G. (2008). Optical Remote Sensing of Glacier Characteristics: A Review with Focus on the Himalaya: Molecular Diversity Preservation International.

Ranzi, R., Grossi, G., Iacovelli, L., & Taschner, S. (2004, 20-24 Sept. 2004). *Use of multispectral ASTER images for mapping debris-covered glaciers within the GLIMS project.* Paper presented at the Geoscience and Remote Sensing Symposium, 2004. IGARSS '04. Proceedings. 2004 IEEE International.

Raup, B. (2010). GLIMS Analysis Tutorial. Retrieved February, 12, 2011, from http://www.glims.org/MapsAndDocs/assets/GLIMS_Analysis_Tutorial_a4.pdf

Robinson, V. (2003). A Perspective on the Fundamentals of Fuzzy Sets and their Use in Geographic Information Systems. *Trans GIS, 7*(1), 3-30.

Shukla, A., Arora, M. K., & Gupta, R. P. (2010). Synergistic approach for mapping debris-covered glaciers using optical-thermal remote sensing data with inputs from geomorphometric parameters. [doi: DOI: 10.1016/j.rse.2010.01.015]. *Remote Sensing of Environment, 114*(7), 1378-1387.

Silverio, W., & Jaquet, J. (2005). Glacial cover mapping (1987-1996) of the Cordillera Blanca (Peru) using satellite imagery. [doi: DOI: 10.1016/j.rse.2004.12.012]. *Remote Sensing of Environment, 95*(3), 342-350.

Stein, A., Hamm, N., & Ye, Q. (2009). Handling uncertainties in image mining for remote sensing studies. *International Journal of Remote Sensing, 30*(20), 5365-5382.

Taschner, S., & Ranzi, R. (2002a, 24-28 June 2002). *Comparing the opportunities of Landsat-TM and Aster data for monitoring a debris covered glacier in the Italian Alps within the GLIMS project.* Paper presented at the Geoscience and Remote Sensing Symposium, 2002. IGARSS '02. 2002 IEEE International.

Taschner, S., & Ranzi, R. (2002b). Comparing the opportunities of LANDSAT-TM and ASTER data for monitoring a debris covered glacier in the Italian alps within the GLIMS project.

Team, A. G. V. (2009). ASTER GDEM Validation Team. Retrieved December, 21, 2010, from http://www.ersdac.or.jp/GDEM/E/image/ASTERGDEM_ValidationSummaryReport_Ver1.pdf

Van de Vlag, D. E., & Stein, A. (2007). Incorporating uncertainty via hierarchical classification using fuzzy decision trees. *Geoscience and remote sensing, 45*(1), 237 - 245.

Whalley, W. B., & Martin, H. E. (1986). The problem of hidden ice in glacier mapping. *Annals of Glaciology, 8*, 181-183.

Zhao, X., Stein, A., & Chen, X. (2009). *A random sets model for spatial objects with uncertain boundaries*. Paper presented at the Proceedings of the 12th AGILE internationational conference on geographic information science.

Zhao, X., Stein, A., & Chen, X. (2010). Application of random sets to model uncertainties of natural entities extracted from remote sensing images. *Stochastic Environmental Research and Risk Assessment, 24*(5), 713-723.

# APPENDIX A – PROBABILITY MAP OF FEDCHENKO

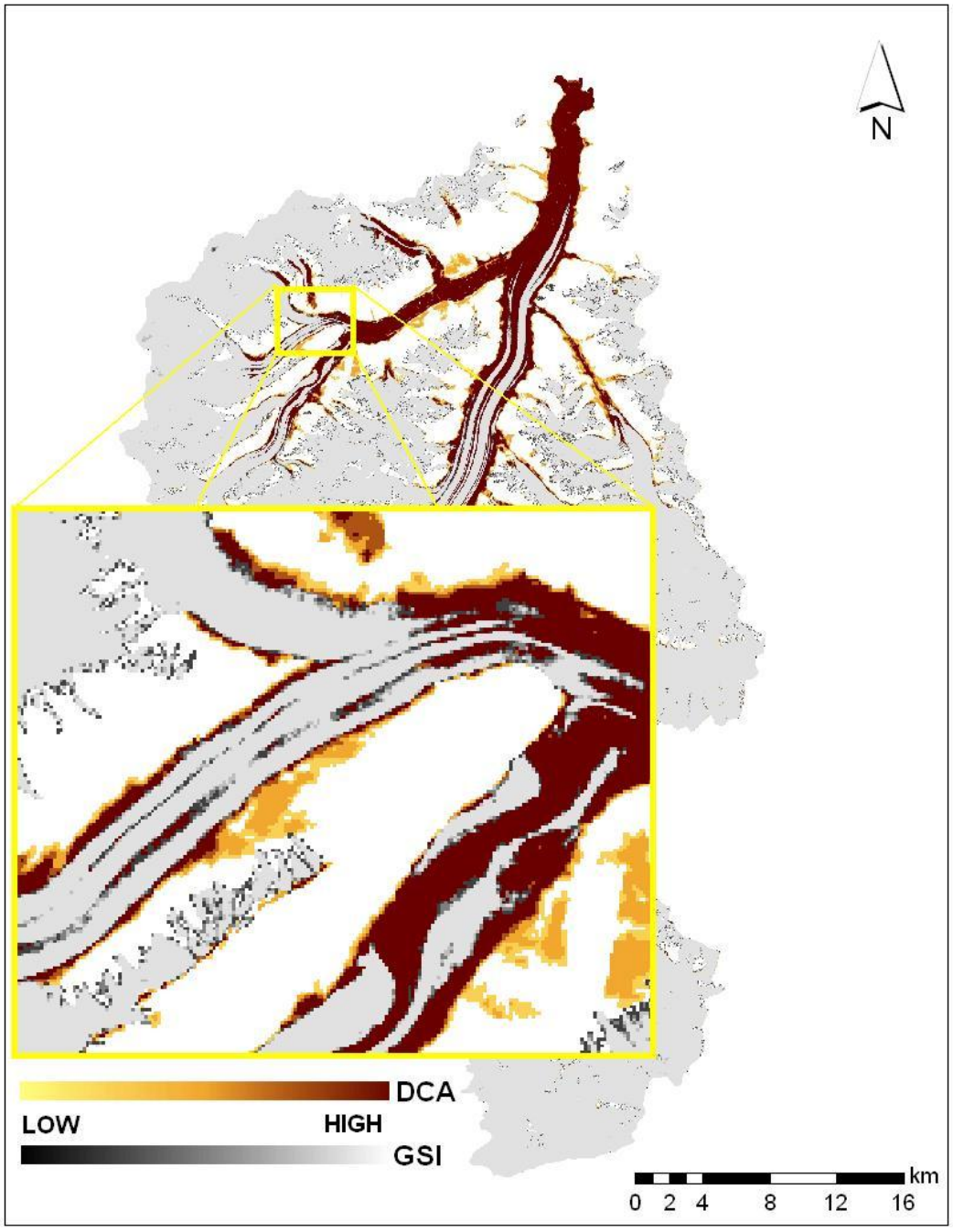


Figure 36. Probability map of Fedchenko glacier (September, 1999)

# APPENDIX B – GLACIER RETREAT

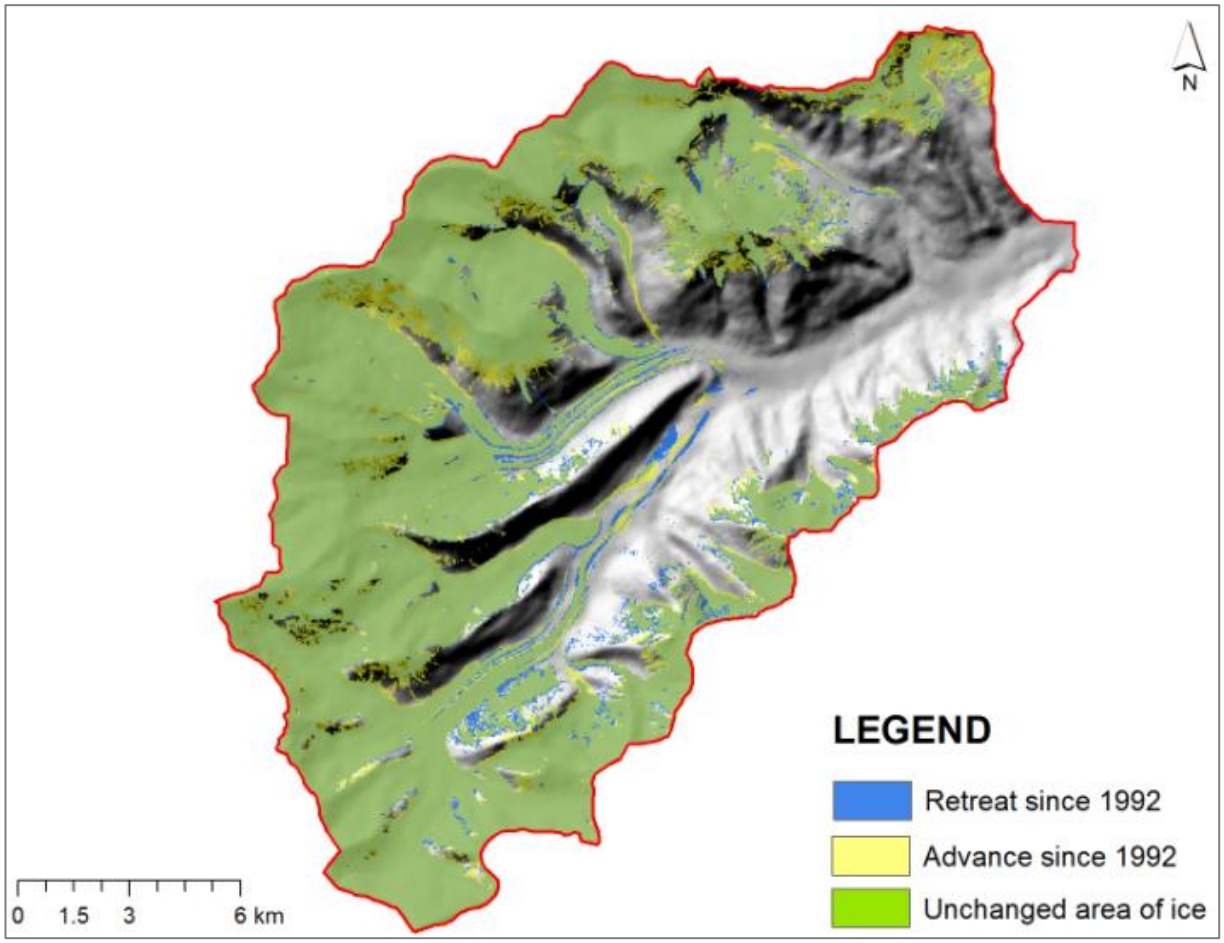


Figure 37. Glacier retreat since 1992